Supergene and exotic Cu mineralization occur during periods of landscape stability in the Centinela Mining District, Atacama Desert

Article *in* Basin Research · July 2017

DOI: 10.1111/bre.12258

CITATIONS
3

READS
298

10 authors, including:

Miguel Tapia
Universidad de Atacama
3 PUBLICATIONS **3** CITATIONS
SEE PROFILE

Eduardo Campos
Universidad Católica del Norte (Chile)
34 PUBLICATIONS **286** CITATIONS
SEE PROFILE

Sebastien Carretier
Institute of Research for Development
105 PUBLICATIONS **1,613** CITATIONS
SEE PROFILE

Rodrigo González
Universidad Católica del Norte (Chile)
57 PUBLICATIONS **52** CITATIONS
SEE PROFILE

Basin Research

IAS EAGE

Basin Research (2017) 1–31, doi: 10.1111/bre.12258

Supergene and exotic Cu mineralization occur during periods of landscape stability in the Centinela Mining District, Atacama Desert

Rodrigo Riquelme,* Miguel Tapia,*,† Eduardo Campos,* Constantino Mpodozis,‡ Sebastien Carretier,§ Rodrigo González,* Sebastian Muñoz,* Alberto Fernández-Mort,*,¶ Caroline Sanchez*,§ and Carlos Marquardt,**

**Departamento de Ciencias Geológicas, Universidad Católica del Norte, Antofagasta, Chile*
†Departamento de Geología, Universidad de Atacama, Copiapó, Chile
‡Antofagasta Minerals, Las Condes, Santiago, Chile
§Géosciences Environnement Toulouse, OMP, UPS, CNRS, IRD, Université Toulouse III, Toulouse, France
¶Departamento de Petrología y Geoquímica, Fac. CC. Geológicas, Universidad Complutense de Madrid, Madrid, Spain
***Departamento de Ingeniería de Minería y Grupo de Geociencias, Pontificia Universidad Católica de Chile, Santiago, Chile*

ABSTRACT

The Centinela Mining District (CMD), Atacama Desert (northern Chile), includes several mid-late Eocene porphyry Cu deposits that contains supergene mineralization and provides access to a record of gravel deposits that host syn-sedimentary exotic Cu mineralized bodies. By studying these gravels, we reconstruct the unroofing history and constrain the geomorphological conditions that produced supergene and exotic Cu mineralization. We present an integrated study based on stratigraphic and sedimentological data, lithology clast counts, $^{40}Ar/^{39}Ar$ and U/Pb ages from interbedded tuff layers and U/Pb detrital zircon geochronology data. To relate the gravel deposition episodes to the timing of the supergene mineralization, we provide in-situ and exotic supergene mineral ages (40Ar/39Ar and K-Ar). Six gravel units were deposited between the mid-Eocene and the mid-Miocene. The Esperanza gravels were deposited concurrently with the emplacement of porphyry Cu deposits at depth. The subsequent Tesoro I, II and III and Atravesado gravels register the unroofing of these deposits, from the advanced argillic zone to the sericitic and prophylitic hypogene zones. The Arrieros gravels register landscape pediplanation, that is, denudational removal and wear of the landscape to base level on a relatively stable tectonic regime, occurring roughly contemporaneous with supergene activity. The supergene mineral ages of the CMD define a time span (*ca.* 25–12 Ma) during which most of the supergene ages cluster in northern Chile. This time span corresponds with a period of warm and humid climate conditions in the southern hemisphere. We conclude that landscape pediplanation favours supergene mineralization and helps preserve the former supergene mineralized zones from significant erosion. Low erosion rates during pediplanation may constitute a necessary condition for the efficiency of the supergene processes in such semi-arid climate.

INTRODUCTION

Porphyry copper deposits (porphyry Cu) are ore bodies made of hypogene sulphides deposited from hydrothermal solutions in convergent tectonic settings at a depth of about 1–2 km (e.g. Sillitoe, 2010; Yanites & Kesler, 2015; Fig. 1). The hydrothermal solutions are supplied by plug-like stocks or dyke swarms and generate an alteration and hypogene mineralization pattern zoned outward from the intrusion. The Atacama Desert is known worldwide for hosting numerous world-class porphyry Cu deposits. The economic wealth of most of these ore deposits relates to the remobilization, within the weathering profile, of the copper originally contained in the hypogene sulphides (Sillitoe & McKee, 1996; Chávez, 2000; Sillitoe, 2005, 2010). Copper remobilization and reprecipitation in the

Correspondence: Riquelme Rodrigo, Facultad de Ingeniería y Ciencias Geológicas, Universidad Católica del Norte, Avenida Angamos 0610, Antofagasta, Chile. E-mail: rriquelme@ucn.cl

supergene environment requires enough groundwater to promote the oxidation and leaching of hypogene sulphides, the transport of copper in solution, the formation of secondary enriched sulphides and/or copper oxide minerals, and eventually the formation of gravel-hosted exotic Cu deposits related to the lateral migration of the solutions (Clark *et al.*, 1990; Münchmeyer, 1996; Chávez, 2000; Sillitoe, 2005; Fig. 1). Two conditions are seen as necessary to generate supergene minerals from the weathering of a porphyry Cu. First, a moderate precipitation rate, at the very least, is required (>100 mm year^{-1}, i.e. a semi-arid climate, Clark *et al.*, 1990), which would provide high water-to-rock ratios that favour supergene mineral generation (e.g. Vasconcelos, 1999; Chávez, 2000). Second, supergene mineralization requires a water table descent rate that allows for the hypogene sulphides to be gradually exposed to the effects of oxidative weathering (Hartley & Rice, 2005; Sillitoe, 2005; Bissig & Riquelme, 2009, 2010). Thus, the average erosion rate must be in overall balance with the water table descent rate so that the sulphides can undergo significant oxidation before they are removed mechanically (e.g. Emmons, 1917; Ransome, 1919; Brimhall *et al.*, 1985; Sillitoe, 2005). The precise climatic and geomorphologic conditions favouring the generation of supergene minerals are a matter of discussion.

The available ages obtained from supergene minerals indicate that the supergene processes affecting ore deposits in the Atacama Desert in northern Chile and southern Peru were active for a period of time between 45 Ma and 6 Ma (e.g. Gustafson & Hunt, 1975; Alpers & Brimhall, 1988; Sillitoe & McKee, 1996; Marsh *et al.*, 1997; Mote *et al.*, 2001; Bouzari & Clark, 2002; Quang *et al.*, 2003, 2005; Arancibia *et al.*, 2006; Bissig & Riquelme, 2010). Some authors postulate that most of the supergene processes began at *ca.* 30 Ma and reached a peak at 14–21 Ma. The lack of ages younger than *ca.* 9 Ma from supergene minerals suggests that supergene activity on ore deposits ended at that time (Mote *et al.*, 2001; Bouzari & Clark, 2002; Arancibia *et al.*, 2006). Other authors point out that a significant number of these ages concentrate at *ca.* 20, *ca.* 14 and *ca.* 6 Ma, which are interpreted as episodes of intense supergene activity (e.g. Alpers & Brimhall, 1988; Sillitoe & McKee, 1996; Reich *et al.*, 2009). Consequently, along with the two conditions needed to generate supergene minerals, two hypotheses have been proposed to explain these supergene episodes. First, they have been related to the prevalence of relatively wetter climate conditions that disrupted the late Cenozoic arid climate history of the Atacama Desert (e.g. Clark *et al.*, 1990; Chávez, 2000; Arancibia *et al.*, 2006). Second, they may have resulted from an episodic water

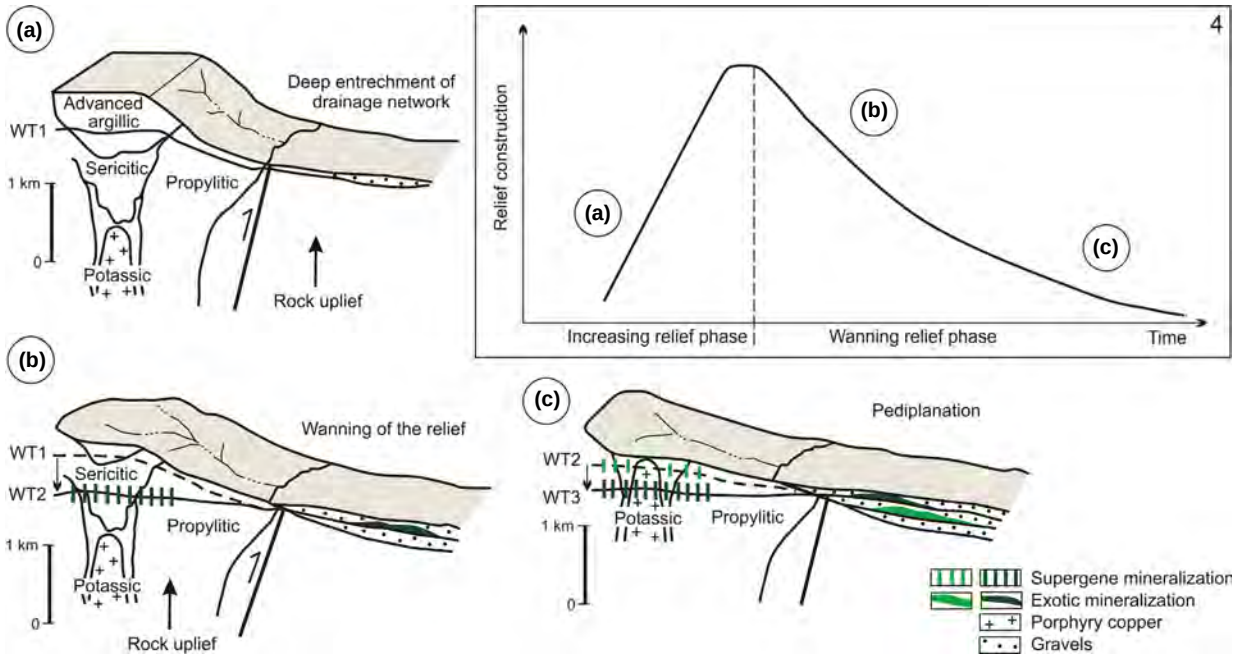

Fig. 1. Conceptual model of the co-evolution of the landscape and porphyry Cu unroofing following a rock uplift episode. The figure shows the generalized hypogene mineralization zoning pattern related to a porphyry Cu deposits and the hypothesized exhumation level in each stage of the landscape evolution. (a) increasing relief stage and deep entrenchment of the drainage network on the advanced argillic hypogene zone. (b) Beginning of the waning of the relief and river incision on the sericitic and propylitic hypogene zone. (c) Pediplanation stage. 4, geomorphological evolution cycle following a main rock uplift episode and the moment in which each mentioned stage occurs. We hypothesize that supergene and exotic Cu mineralization may result from the descent of the water table driven by river incision, or may occur later, when the landscape pediplanation allows a thick weathering profile to develop.

table descent driven by tectonically triggered unroofing episodes in porphyry Cu (Tosdal, 1978; Anderson, 1982; Brimhall *et al.*, 1985; Clark *et al.*, 1990; Bouzari & Clark, 2002; Quang *et al.*, 2003; Hartley & Rice, 2005; Sillitoe, 2005). The scarcity of supergene mineral ages older than the early Oligocene is interpreted as the result of rapid erosion linked to the Incaic tectonic phase, which precludes the preservation of supergene oxidation profiles (Arancibia *et al.*, 2006). The lack of younger supergene mineral ages is considered to be due to the middle Miocene climate change from arid to hyperarid conditions, which limited the supergene alteration processes and favoured the preservation of previously formed supergene mineralized zones (e.g. Alpers & Brimhall, 1988; Sillitoe & McKee, 1996; Bissig & Riquelme, 2009, 2010).

Although the time frame for the supergene processes is relatively well constrained, the geomorphological evolution cycle following a main rock uplift episode has not yet been considered. Unroofing occurs at different rates throughout a period of time which may encompass more than 10 Ma following the main rock uplift period, particularly in arid regions. In the Atacama Desert, this time span corresponds to the response time of mountain erosion which leads towards the formation of a smooth, gently sloping (<10°), low relief landscape surface commonly called pediplain (e.g. Mortimer, 1973; Riquelme *et al.*, 2003, 2007; Farías *et al.*, 2005; Aguilar *et al.*, 2011; Rodriguez *et al.*, 2013). Pediplains result from denudational removal and wear to near base level, acting during a period of long tectonic stability at the end of a Davis′s cycle of erosion (Davis, 1905; for synthesis see Phillips, 2002; Strudley & Murray, 2007; Dohrenwend & Parsons, 2009). The landscape evolution usually begins with a deep entrenchment of the drainage network, followed by a waning of the relief due to prolonged sub-aerial erosion, eventually associated with a parallel retreat of the initial topographic front (pediplanation) (e.g. Phillips, 2002; Strudley & Murray, 2007; Carretier *et al.*, 2014; Fig. 1). The precise moment during the geomorphological evolution cycle of an uplifted landscape at which the appropriate balance between erosion rate and the water table descent rate takes place has still not been clarified (Mortimer, 1973; Alpers & Brimhall, 1988; Bouzari & Clark, 2002; Quang *et al.*, 2003; Bissig & Riquelme, 2010). Two cases favouring this type of balance exist: supergene processes may result from the descent of the water table driven by river incision, thereby exposing the underlying sulphides to the effects of oxidative weathering (e.g. Bissig & Riquelme, 2009, 2010; Fig. 1b), or it may occur much later, when the lowering of the relief reduced the erosion rate and allowed a thick weathering profile to develop (Fig. 1c). One of the main goals of the present work is to understand this issue.

The Incaic tectonic phase is an important episode of erosion and denudation in the Precordillera that occurred during and immediately after the mid-late Eocene emplacement of the porphyry Cu in northern Chile (e.g. Maksaev & Zentilli, 1999). This phase and the subsequent geomorphological evolution and paleoclimatic history of the Precordillera results in semi-consolidated gravel deposits – the Atacama Gravels (Mortimer,1973) – which cover most of the Central Depression and the Precordillera (e.g. Sáez *et al.*, 1999, 2012; Hartley & Chong, 2002; Hartley, 2003; Lamb & Davis, 2003; Dunai *et al.*, 2005; May *et al.*, 2005; Rech *et al.*, 2006, 2010; Riquelme *et al.*, 2007; Nalpas *et al.*, 2008; Amundson *et al.*, 2012; Jordan *et al.*, 2014; de Wet *et al.*, 2015; Oerter et al., 2016). We consider the Centinela Mining District (CMD), which provides unusual access to a complete record of mid-Eocene to mid-Miocene gravel deposits in which mineralized exotic Cu bodies are hosted. The district also exposes several porphyry Cu deposits affected by supergene mineralization, in which the ages of the hypogene mineralization are well constrained (Perelló *et al.*, 2010; Mpodozis & Cornejo, 2012). The gravel deposits of the CMD potentially provide a picture of the tectonic episodes, the geomorphologic and paleoclimatic conditions in which the supergene processes occurred. In this work, we describe the sedimentary facies and stratigraphy of the gravel deposits and provide geochronological constraints of the age of their deposition. Detrital zircon geochronological data combined with clast counts are used to reconstruct the unroofing sequence of the porphyry Cu deposits. To relate the supergene mineralization episodes with the timing of the gravel deposition, we provide supergene and exotic Cu mineral ages, which complement the ages previously reported in the CMD.

This study is one of the few works dedicated to understand the geomorphological condition that controls supergene mineralization, in an area where geologists are intensively searching for signals in the sedimentary record that may help find copper deposits hidden by the mid-Eocene to mid-Miocene gravel cover. The main questions addressed in this contribution are as follows: Can the unroofing history of the porphyry Cu be reconstructed from the mid-Eocene to mid-Miocene gravel record of the CMD? How did this history control the supergene mineralization episodes and exotic Cu deposition? Can the supergene mineralization be related to a specific event during the unroofing process or is it linked to a particular geomorphological setting and/or to a specific paleoclimatic episode?

GEOLOGICAL SETTING

The CMD is located in the Antofagasta Region of northern Chile, *ca.* 40 km SSW of Calama city and includes several mid-late Eocene porphyry Cu deposits (Mirador, Esperanza, Esperanza Sur, Encuentro, Penacho Blanco and Polo

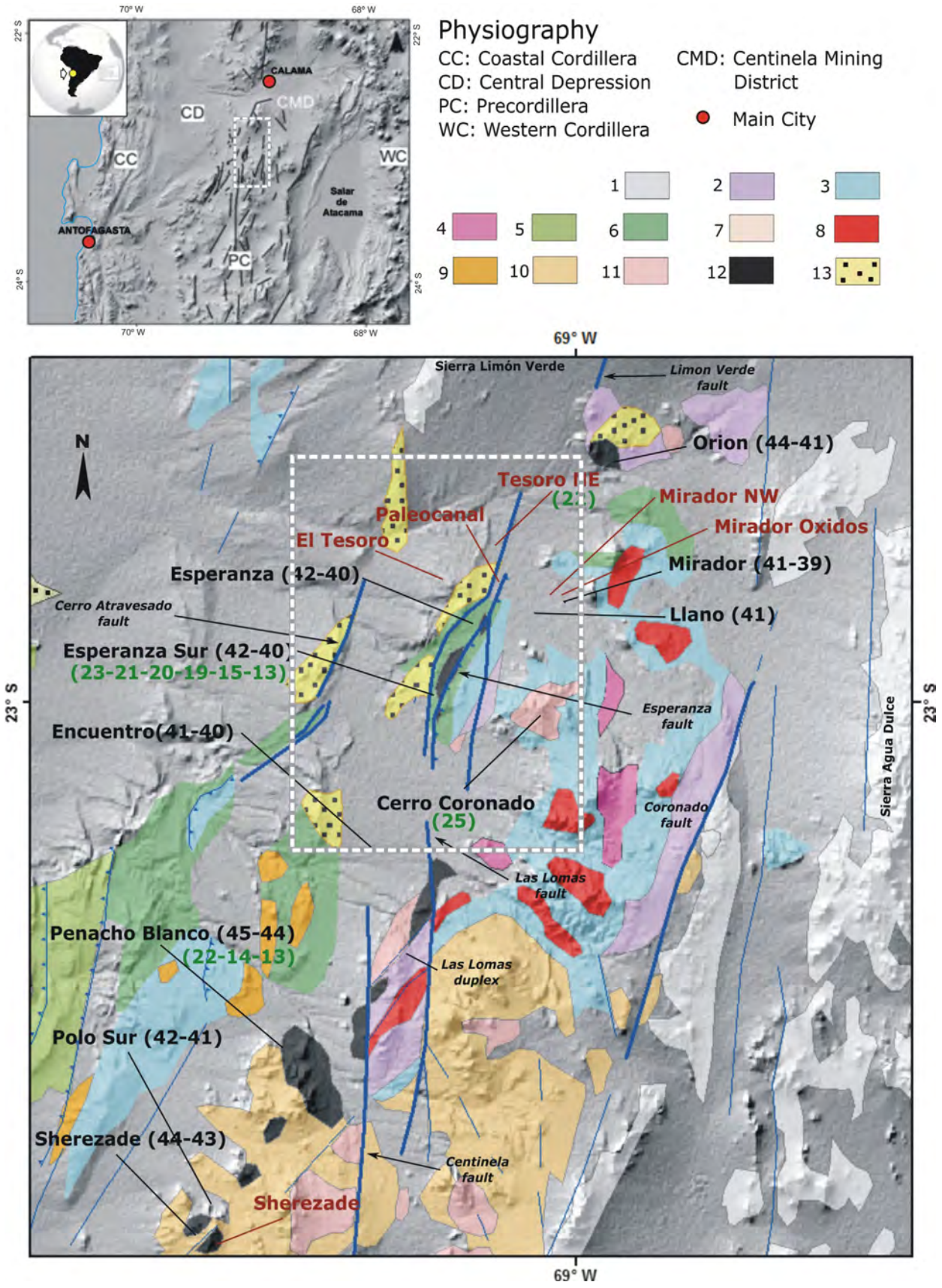

Fig. 2. (a) Location of the Centinela Mining District and the physiographic setting of the Atacama Desert in the Antofagasta Region of northern Chile. The main structures of the Domeyko Fault System in the Precordillera are shown. (b) Regional geological map of the CMD showing the main mineralized porphyry systems (taken from Mpodozis & Cornejo, 2012). 1, Upper Paleozoic (290–270 Ma) basement. 2, Upper Triassic (210–200 Ma) volcanic and sedimentary rocks. 3, Jurassic to Lower Cretaceous sedimentary and volcanic rocks. 4, Lower Cretaceous (124–100 Ma) gabbros to diorites and granodioritic porphyry intrusions. 5, Lower Cretaceous (?) volcanic rocks. 6, Upper Cretaceous (78–66 Ma) sedimentary and volcanic succession (Quebrada Mala formation).7, Undifferentiated Cretaceous granitoids. 8, Late Cretaceous (78–68 Ma) diorites and (minor) rhyolitic porphyry intrusions. 9, Lower Paleocene (65–64 Ma) diorites and dacitic porphyry intrusions. 10, Paleocene to Lower Eocene (64–53 Ma) volcanic rocks (Cinchado formation). 11, Paleocene (60–56 Ma) monzodiorites and rhyolitic porphyry intrusions. 12, Late Eocene (44–40 Ma) monzodioritic to granodioritic stocks and mineralized dacitic porphyry intrusions. 13, Upper Eocene to Oligocene gravel units (Esperanza, Tesoro I, Atravesado I and II in this work). Numbers in black corresponds to U/Pb zircon emplacement ages yielded by porphyry Cu intrusions. Numbers in green indicate the supergene mineral ages reported in this work (see Table 3).

Sur), all of which belong to the porphyry copper belt of northern Chile (Perelló *et al.*, 2010; Mpodozis & Cornejo, 2012; Fig. 2). Porphyry Cu mineralization in the district occurs along the western border of the Cordillera de Domeyko (or Precordillera), an uplifted basement range essentially formed by late Paleozoic to Triassic volcanic and intrusive rocks with ages between 320 and 200 Ma including, at Sierra Limón Verde (Fig. 2b), minor outcrops of Neoproterozoic to Paleozoic sedimentary and metamorphic units (Marinovic & García, 1999; Basso & Mpodozis, 2012; Morandé, 2014). The Cretaceous to Eocene geological evolution of the CMD records a lengthy history of magmatic activity. The oldest plutonic rocks correspond to a group of Early Cretaceous gabbros and quartz diorites, with U/Pb zircon ages between 122 and 116 Ma (Cornejo & Mpodozis, 2015). These plutonic rocks were emplaced within Upper Triassic (210–200 Ma) volcanic and sedimentary rocks (Estratos Las Lomas) and within Jurassic to Lower Cretaceous fossiliferous marine rocks and evaporites (Caracoles Group; Marinovic & García, 1999). All of the previously mentioned units are unconformably covered by an Upper Cretaceous (78–66 Ma) succession including andesitic lavas and breccias and sedimentary rocks from the Quebrada Mala Formation (Marinovic & García, 1999). This succession is in part coeval to a group of diorites to rhyolite porphyries and flow domes, with U/Pb zircon ages between 70 and 66 Ma (Mpodozis & Cornejo, 2012). Volcanism continued into Cenozoic time with the deposition of the Cinchado Formation, a volcanic succession that includes basaltic to andesitic lava flows and rhyolitic ignimbrites and domes (Mpodozis & Cornejo, 2012). These volcanic rocks derived from stratovolcanoes and small collapse calderas that were active between the early Paleocene (64 Ma) and the early Eocene (53 Ma). During this interval, a diverse group of epizonal intrusions containing quartz diorite to monzodiorite (60 Ma) and granodiorite (58–57 Ma) plus andesitic to dioritic porphyritic intrusions were emplaced in the Mesozoic units and Paleogene volcanic edifices (Mpodozis & Cornejo, 2012).

Mineralized porphyry Cu intrusions were emplaced in the CMD between 45 and 39 Ma (U/Pb zircon data; Perelló *et al.*, 2010; Mpodozis & Cornejo, 2012). The porphyries mainly correspond to hornblende-biotite dacite dike swarms that, together with several barren pyroxene-hornblende dioritic stocks and lacoliths, form a 40-km long, N to NE-trending belt, which includes at least 10 discrete intrusive complexes. The oldest porphyry Cu (45–43 Ma) deposits were emplaced on the southwestern end of the belt, with the ages decreasing northeastward, reaching 39 Ma at the northeastern edge of the porphyry belt (Fig. 2b). The hypogene mineralization in the district has been dated by $^{40}Ar/^{39}Ar$ and K-Ar hydrothermal biotite and Re-Os molybdenite ages between 45 and 40 Ma and is related to the above-mentioned dike swarms (Perelló *et al.*, 2010). Exotic Cu mineralization derived from supergene copper leaching of the hypogene sulphides contained in nearby porphyry Cu deposits can be recognized in the Paleocanal, El Tesoro and Tesoro NE deposits (Mora *et al.*, 2004; Perelló *et al.*, 2010).

The main structural feature of the CMD is a 3–5 km wide, N-S trending fault zone, which includes the Atravesado, Centinela, Las Lomas, Esperanza and Coronado faults, and that cuts obliquely across the porphyry Cu belt (Fig. 1b). This fault zone is part of the Domeyko Fault System (DFS), a major zone of tectonic deformation stretching for >1000 km along the Precordillera of northern Chile (Mpodozis *et al.*, 1993). The main episode of tectonic activity along the DFS seems to have occurred between the mid-Eocene to early Oligocene (45–33 Ma, the Incaic tectonic orogeny; Maksaev & Zentilli, 1999; Tomlinson *et al.*, 2001; Arriagada *et al.*, 2008). Porphyry Cu-related intrusions, which represent the most relevant metallogenic episode in northern Chile, are associated with the Incaic tectonic orogeny (Mpodozis & Perelló, 2003; Sillitoe & Perelló, 2005). The Incaic tectonic orogeny is also an important episode of exhumation in the Domeyko Cordillera as evidenced by fission-track data (Maksaev & Zentilli, 1999; Nalpas *et al.*, 2005; Sanchez *et al.*, 2015). However, the detailed kinematic history of the DFS is a matter of controversy as evidence for both left- and right-lateral displacement, including reversal displacements, has been documented along discrete faults that form the system (Reutter *et al.*, 1996; Tomlinson & Blanco, 1997a,b; Niemeyer & Urrutia, 2009; Dilles *et al.*, 2011).

At the CMD, the erosion and denudation of the Domeyko Cordillera in response to the Incaic tectonic orogeny resulted in the deposition, between the mid-late Eocene to the mid-Miocene, of up to *ca.* 800 m of gravel and sand deposits with scarce interbedded volcanic and evaporite layers. The upward stratigraphic sedimentary changes of these deposits are probably controlled by tectonic episodes and climatic fluctuations. Likewise, the upward stratigraphic changes in the clast composition potentially record the unroofing history for the porphyry Cu emplaced in the Domeyko Cordillera at this area. The sedimentary, clast composition and detrital zircon changes across these deposits are presented herein.

GRAVEL UNITS OF THE CMD

We identified seven gravel units along the CMD on the basis of contact relationships, sedimentary facies, lithology of clasts and the presence of interbedded volcanic layers. The surface distribution and sedimentological information of the gravel units were collected during a 1:25.000 mapping of the CMD, which focused on the gravel record (Fig. 3). Sedimentological information was also collected from six stratigraphic columns measured on a centimetre to meter scale (Fig. 4). The sedimentary facies were described using the criteria proposed by Miall (1996) and Hogg (1982) and the modifications used for the gravel deposits in the Atacama Desert by Blanco & Tomlinson (2002) and Nalpas *et al.* (2008) have also been considered (Table 1). Once familiarized with the sedimentary facies, we were able to differentiate between the gravel units on two drill cores (>700 m of cores) that were provided by the Antofagasta Minerals S.A. mining company (Fig. 5). The sub-surface distribution was defined based on drill core logging and the sub-surface geological and structural information reported by Mpodozis & Cornejo (2012). Based on this information, geological profiles oriented across the main structural features were constructed (Fig. 6). Previous work done in the area defines an informal stratigraphy for the Tesoro mine area (Blanco & Tomlinson, 2002; Mora *et al.*, 2004; Tapia *et al.*,

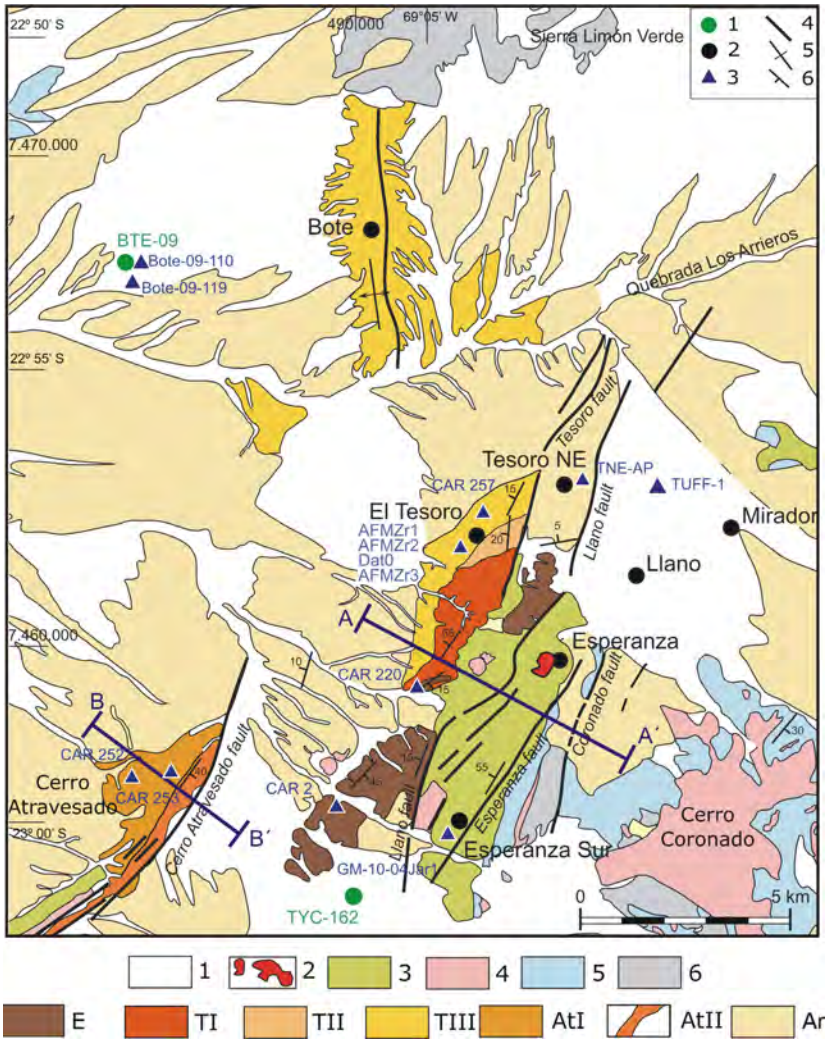

Fig. 3. Geological map focused on the mid-Eocene to mid-Miocene gravel deposits in the CMD. E: Esperanza gravels, TI, II and III: Tesoro I, II and III gravels, respectively, AtI and II: Atravesado I and II gravels, respectively, Ar: Arriero gravels. The figure shows the names of the localities and the drill holes discussed in the text. Symbols: 1: drill hole, 2: open mine pits, 3: location of the geochronological data, 4: Faults, 5: Anticline, 6: Dip bed. Legend. 1: Post-mid-Miocene poorly consolidated gravel deposits constituting the alluvial fans observed on the landscape surface. 2: Eocene (45–39 Ma) mineralized porphyry intrusions. 3: Upper Cretaceous sedimentary and volcanic rock. 4: Cretaceous and Paleocene intrusions. 5: Jurassic to Lower calcareous rocks. 6: Upper Paleozoic and Triassic basement. AA′ and BB′ show the location of the geological profile in Figure 6.

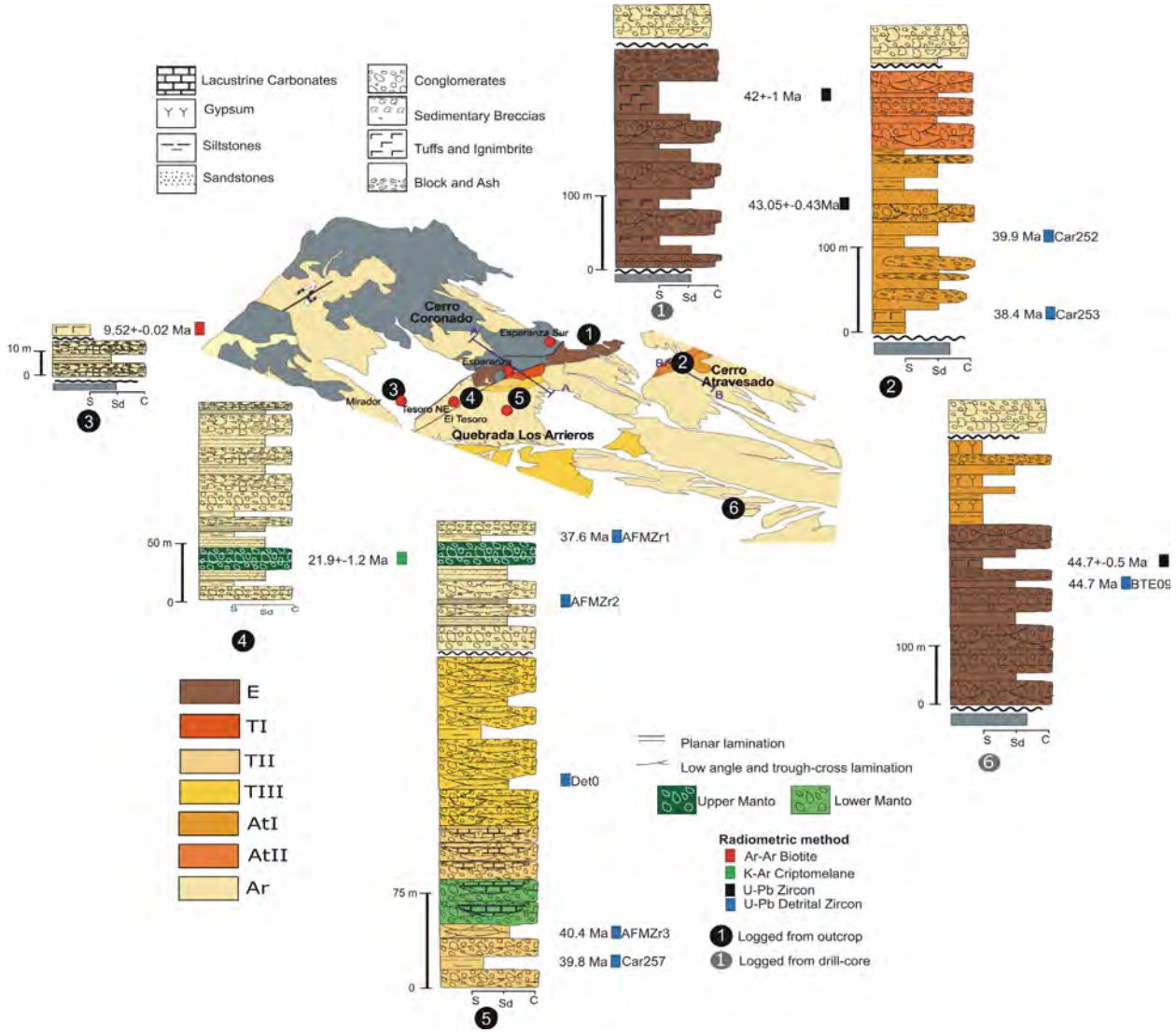

Fig. 4. Stratigraphic columns used to study the mid-Eocene to mid-Miocene gravel deposits. The columns were constructed either from outcrops or from drill core logging. The location of the columns is shown on a towards-the-south 3D view of the map presented in Fig. 3 (with the pre-Eocene rocks simplified as a grey colour). The columns also show the stratigraphic position of the geochronological data discussed in the text. The stratigraphic positions of the recognized exotic Cu mantos are shown. Note that the vertical scale changes between the columns. The abbreviations of gravel units are given in Fig. 3.

2012). The equivalence between the gravel unit names used by these authors and the names used in this work is shown in Table S1.

Esperanza gravels

Sedimentology

The Esperanza Gravels are composed of Gh and Gpt facies with sporadic intercalations of Sm, Fsm and rare Gmm facies, and abundant intercalations of volcanic layers (Fig. 5a,b). The Gh and Gpt facies are well rounded, mainly cobble grade, normally imbricated, and form tabular elongated bodies that extend by several tens of meters, with a meter-scale thickness (2–7 m). The Sm and Fsm intercalations form tabular continuous, centimetric-scale thick bodies. The volcanic intercalations include interbedded rhyolitic and dacitic, poorly consolidated, tuff layers and block and ash deposits.

Distribution and stratigraphic relationship

The outcrops of this gravel unit are restricted to the Esperanza Sur area and the area between Esperanza and Tesoro NE. In the Esperanza Sur area, it is composed of brown-reddish coloured strata and forms an open syncline with an NE-SW-oriented axis (Fig. 3).

Table 1. The facies codes are modified from Miall (1996) and consider the modifications used for the gravel deposits in the Atacama Desert by Blanco & Tomlinson (2002) and Nalpas *et al.* (2008).

Facies	Description	Depositional Processes
Gmm: Matrix-supported, massive gravels.	Sub-rounded to sub-angular, ungraded and poorly sorted gravels, granule to cobble grained. Occasionally clast imbrication.	Cohesive flow deposits, sub-aerial to sub-aqueous debris flows (Smith, 1986; Miall, 1996).
Gcm: Clast-supported, massive gravels.	Rounded, sub-rounded to sub-angular, ungraded and poorly sorted gravels, granules to boulders, coarse sandy matrix.	Plastic or pseudo-plastic hyper-concentrated density flows, resulting from high sediment and water discharge floods with rapid transport and deposition (Waresback and Turbeville, 1990; Svendsen *et al.*, 2003; Smith, 1986; Horton and Schmitt, 1996).
Gh: Clast-supported, horizontally laminated gravels.	Sub-rounded to sub-angular gravels. Granules to cobble. Imbrication and flattened clast alignments	Longitudinal bar or lag deposits that result from channelized streamfloods under upper-flow regime conditions (Waresback and Turbeville, 1990; Miall, 1996). Deposited from high energy, bedload tractive, unconfined or poorly confined sheetfloods (Nemec and Steel, 1984; Horton and Schmitt, 1996; Nalpas *et al.*, 2008).
Gpt: Planar and trough cross-bedded gravels.	Clast-supported gravels. Sub-rounded to sub-angular gravels. Granules to Pebble. Imbrication.	Channel infill deposits related to transverse and lingoid bars or with 2D–3D dunes, deposited in the upper part of lower flow regime conditions (Miall, 1996; Bordy and Catuneanu, 2001; Uba *et al.*, 2005).
Sm: Massive sand.	Ungraded and unstratified fine to coarse sand with scattered gravel clasts.	Hyper-concentrate flows (Smith, 1986) or high-density turbidity currents when the sand deposition is too rapid to allow the development of bedforms (Horton and Schmitt, 1996).
Sh: horizontally laminated sand.	Fine to coarse well-sorted sand with scattered gravels. Planar or sub-planar lamination.	Deposited from high energy, sheetfloods or sheetflows in the lower part of the upper-flow-regime conditions (Collinson, 1996; Miall, 1996).
Spt: Planar and trough cross-stratified sand.	Planar and trough cross-bedded sands with scattered gravels.	Stream flow deposits associated with transverse and lingoid bars or with 2D–3D dunes, under lower flow-regime conditions (Miall, 1996; Bordy and Catuneanu, 2001; Uba *et al.*, 2005).
Fsm: Silt, mud and very fine sand,	Massive or poorly laminated, scattered sub-angular to sub-rounded gravel clasts	Confined flows in a shallow-water environment or sub-aerial waning flood flows (Miall, 1977; Horton and Schmitt, 1996).
Fl: horizontally laminated sands and silts	Well-laminated sands and silts. Occasionally soft loading features.	Suspension fallout on stagnant water bodies (Miall, 1996).
Y: massive gypsum	Massive gypsum, indurated with scattered very fine to fine sand clasts.	Salt precipitation under high evaporitic conditions
C: sandy carbonates	Poorly laminated, carbonate cemented sands. Occasionally soft loading features.	Precipitation of primary micrite in stagnant shallow lakes or pond with terrigenous inputs (Fernadez-Mort *et al.*, 2015)

The top of the exposed succession includes a massive, block and ash deposit, and biotite-hornblende-quartz lapilli and crystalline tuffs. In the southward prolongation of the syncline axis, the drill hole core TYC-162 shows that the Esperanza gravels are >300 m thick (Fig. 4, column 1). To the east, the Esperanza gravels are separate from the Upper Cretaceous strata by the sub-vertical Llano Fault. Between the Tesoro NE and Esperanza Sur areas, the Triassic-Upper Cretaceous strata form a long-wavelength asymmetric anticline, which host the 42–40 Ma Esperanza and Esperanza Sur porphyry copper intrusions (Fig. 6a). The frontal

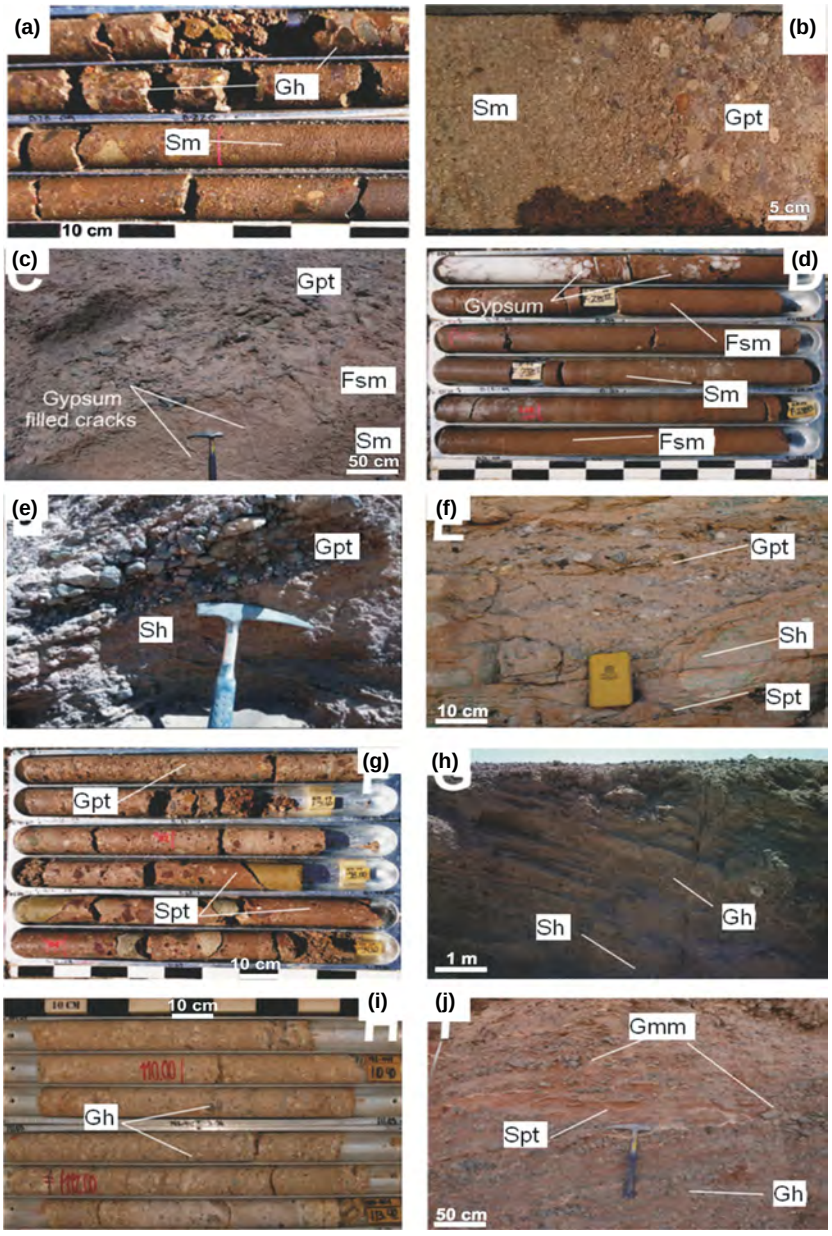

Fig. 5. Some of the main sedimentary features differentiating the gravel units (see Fig. 3 for the locations). (a, b) sedimentary features identified in the Esperanza gravels from drill core BTE-09. (c, d) Sedimentary features identified in the Atravesado I gravels in the Atravesado area and from drill core BTE-09, respectively. (e) Sedimentary features identified in the Atravesado II gravels in the Atravesado area. (f, g) Sedimentary features identified in the Tesoro II gravels from the benches of the Tesoro pit and from a drill core done at the pit bottom, respectively. (h, j) Sedimentary features identified in the Arrieros gravels from the homonymous quebrada and I from drill core BTE-09.

limb of the anticline is upthrown westward along the Telegrafo fault, over the Esperanza gravels. The hinge zone of the anticline and the Esperanza gravels are, in turn, sliced by the Llano sub-vertical fault. To the west, the logging of the drill core BTE_09 shows *ca.* 280 m of mainly Gh and Gpt facies with pyroclastic intercalations, which represents the westernmost evidence of this gravel unit (Figs 3 and 4, column 6).

The Tesoro I gravels

Sedimentolgy

This gravel unit is made of Gcm and Gmm facies, with uncommon Sm and Gh intercalations. These facies form planar to irregular, diffusely based beds measuring several meters thick (1–5 m). The Gcm facies are mainly moderately to poorly sorted and include well-rounded and imbricated clasts, commonly exposing two clast sizes (4–15 cm and 20–40 cm). The Gmm facies are poorly sorted and include sub-angular to sub-rounded, pebble to boulder clasts (large-sized clasts up 30 cm). The Sm facies are coarse-grained and commonly include granule to cobble grained clasts. The Gh facies intercalations are occasionally erosive-based.

Distribution and stratigraphic relationship

This gravel unit outcrops south of the Tesoro mine forming a 10 km long NNE-SSW trending belt in

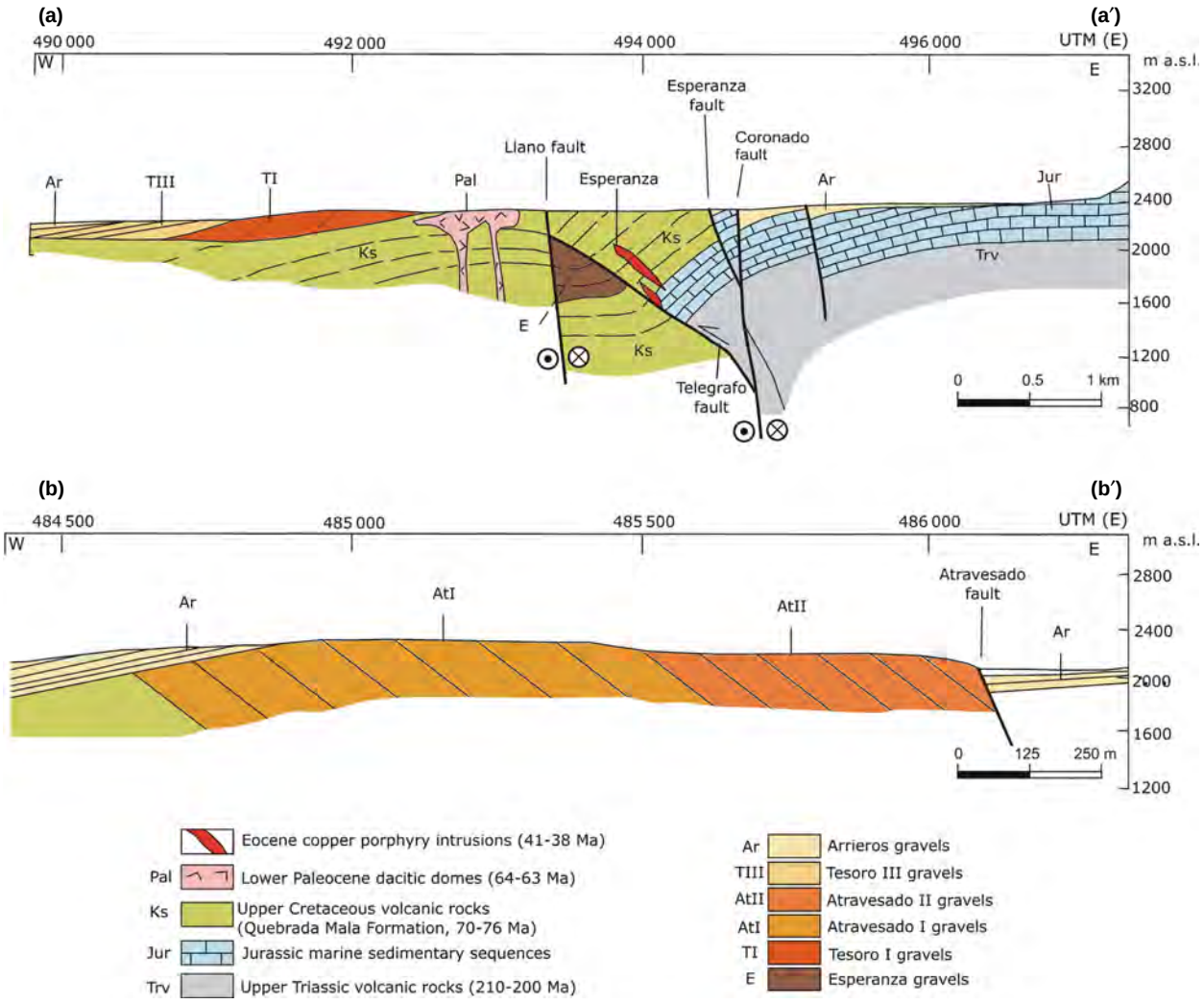

Fig. 6. Geological profiles oriented perpendicular to the main structural features of the Centinela district. Profile AA′ was published by Mpodozis & Cornejo (2012; see page 343) and was constructed from data yielded by an intensive drilling program during which the unexposed Telegrafo Fault was discovered. We slightly modified the profile only adding the gravel units. The location of the profiles is indicated in Fig. 3. Note that the horizontal scale changes between the profiles.

which the beds dip 60–65° NW. It constitutes a light brown to light grey coloured, partially lithified, sedimentary succession that reaches a thickness of *ca*. 400 m. This sedimentary succession unconformably overlays the Upper Cretaceous strata and the Esperanza gravels.

The Tesoro II gravels

Sedimentology

This gravel unit is mainly formed by Gpt facies with common Spt, Sh, Fl and minor C facies intercalations (Fig. 5f,g). The Gpt facies are sub-angular to sub-rounded and form m-scale (1–2 m) erosive-based, lenticular beds that are several meters wide. They are poorly sorted, pebble to boulder grained (2–15 cm in diameter, occasionally up to 30 cm), and locally show clast imbrications. The Spt and Sh facies are medium to coarse-grained and are disposed in lenticular to tabular beds, 0.2–0.4 m thick and several meters wide. The Fl facies forms tabular beds, 0.3–1 m thick and commonly presents cm-scale intercalations of Sh facies. The C sandy carbonate facies, which are described in detail in the work of Fernández-Mort *et al*. (2016), are present as tabular beds that are 0.5–2 m thick and several meters wide. They show very incipient parallel laminations. Carbonate is primarily represented by micrite with a high percentage of fine-grained terrigenous input. The Fl and C facies occasionally expose load casts structures, especially when they underlay coarse-grained beds.

Distribution and stratigraphic relationship

This gravel unit is a light brown coloured, carbonate cemented sedimentary succession that forms a *ca.* 1 km long NE-SW-oriented lenticular outcrop exposed in the Tesoro mine area (Fig. 3). This lenticular body is cut by the Tesoro Fault in its NE limit and is wedged towards the SW. The Tesoro II gravels unconformably overlay the Tesoro I gravels. The most complete sedimentary record of this gravel unit is observed in the Tesoro mine pit, where it reaches up to *ca.* 100 m thick and is composed by beds that dip 10°W and (Figs 3and 4, column 5 Fig. 7b).

The Tesoro III gravels

Sedimentology

This gravel unit is almost completely formed by planar-based, medium- to coarse-grained Gh facies, which forms beds with thickness that varies between 1 and 10 meters. The bedding is mainly given by grain-size changes, occasionally related to cm-scale pebble sand intercalations or by clast alignments. The beds are poorly to moderately sorted and include angular to sub-angular, frequently imbricated clasts (2–10 cm in diameter, occasionally up to 25 cm).

Distribution and stratigraphic relationship

This gravel unit is a red to orange coloured, hematite–limonite–gypsum cemented sedimentary succession that forms a *ca.* 3.5 km long NE-SW-oriented belt that extends from the Tesoro mine towards the SW. In this area, the Tesoro III gravels reach up to 90 m thick; they unconformably overlay the Tesoro I gravels and conformably overlay the Tesoro II gravels. This facies association also forms a north-south trending ridge that extends from Quebrada Los Arrieros to the north (Fig. 3).

The Atravesado gravels

Sedimentology

The lowermost *ca.* 200 m of the column of this gravel unit is made up of Sm, Fsm and Gmm, Gcm facies, with frequent, although variable in proportion (depending on the observed section), intercalations of Gh and Sh facies (Fig. 5c,d). The Gmm, Sm and Gcm facies almost exclusively form planar to irregular, diffuse-based beds. The Sm and Fsm facies are moderately to poorly sorted, and commonly include large-sized scattered clasts (granules to cobbles, rarely boulders). The thicknesses in these facies vary from 1–3 to 18 m. Thin intercalations of Fsm beds frequently expose mudcracks and gypsum veins (Fig. 5c). The Gmm and Gcm facies are several tens of centimetres thick, very poorly to poorly sorted, sub-angular to sub-rounded and commonly granule to cobble grained (large-sized clasts up to 30 cm). The Gh and Sh normally form 1 to 6 m thick successions, and are either on erosive paleo-channel surfaces (1–1.5 m deep, up to 4 m wide) or on diffuse planar surfaces. The Gh are commonly moderately to well sorted, sub-angular to sub-rounded, and include horizontally aligned flattened clasts.

The uppermost *ca.* 100 m of the column of this gravel unit is formed by alternations of Gh, Sh, Gpt and Spt, with minor intercalations of Sm, Fsm and Gcm beds. The Gh, Gpt, Sh and Spt facies fill paleo-channel erosive surfaces, *ca.* 1 m deep and 3–4 m wide (Fig. 5e); however more rarely, the Gh facies can reach up to 6 m thick. The Sm and Gcm facies form lenticular bodies, 50 cm thick and <1 m wide. The Gh facies are moderately to poorly sorted, sub-rounded to rounded, granule to cobble grained (4–7 cm) and commonly show horizontally aligned flattened clasts. The Gpt facies are moderately sorted, rounded to well-rounded granules (1–2 cm) or occasionally cobble grained, normally showing imbricated clasts. The Gcm facies are very poorly sorted, granule to cobble grained (larger-sized clasts of up to 20 cm) and comprise sub-angular to sub-rounded clasts embedded in a silty to fine sand grained matrix. The sand and silt facies are moderately sorted, sub-angular to sub-rounded. The Sm and Fsm facies include dispersed granules, and occasionally cobble gravel clasts.

Distribution and stratigraphic relationship

The Atravesado gravels form a red coloured, carbonate cemented, sedimentary succession exposed in the Atravesado range. It reaches a thickness of *ca.* 300 m and forms an 8 km long NNE-SSW trending belt in which the beds dip 30–40° SE (Figs 3 and 4, column 2). The Atravesado gravels unconformably overlie the Cretaceous Quebrada Mala Formation. A carbonate cemented sedimentary succession mainly formed by Sm and Fsm facies with scarce Gmm facies, which can be attributed to the Atravesado gravels, is recognized as forming the uppermost 120 m of drill core BTE-09 (Figs 3 and 4, column 6).

The Arriero gravels

Sedimentology

This gravel unit is composed of Gh, Sh and minor Gpt and Fl facies, and rarely Gmm and Y facies (Fig. 5h,i,j). The Gh and Gpt facies are composed of poorly to moderately sorted granules to fine pebbles, and angular to sub-rounded clasts. These facies, as well as the Sh facies, form tabular to very elongate lens-shaped, planar-based beds that are tens of centimetres thick. In the Gh facies, the

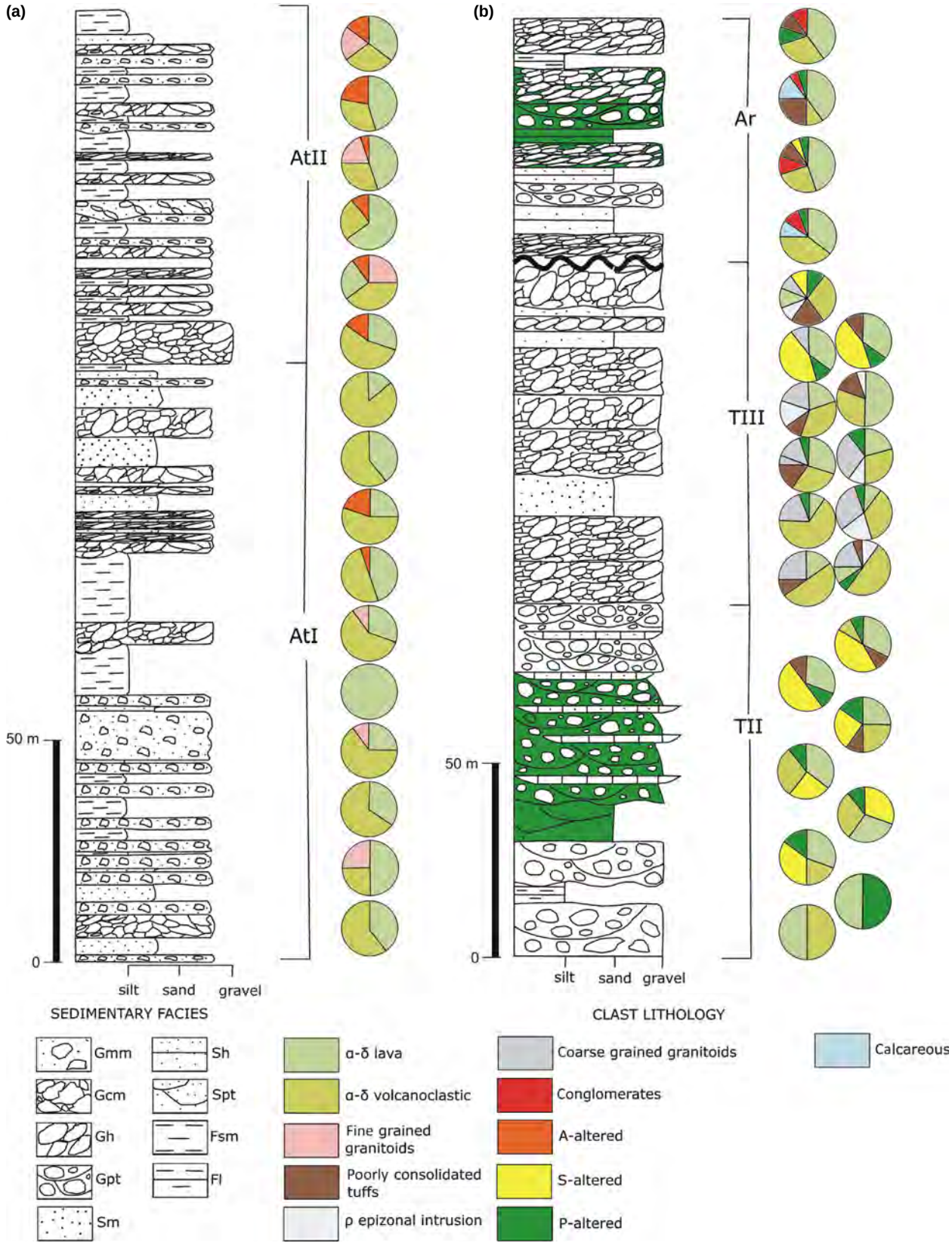

Fig. 7. High-resolution stratigraphic columns (centimetre to meter scales) showing the clast counts performed in this work. (a) column logged for the Atravesado I and II gravels in the Atravesado area (column 2 in Fig. 4). (b) stratigraphic column logged for the Tesoro II and III and the Arrieros gravels in the Tesoro open pit (column 5 in Fig. 4).

lamination is given by grain-size changes or by flattened clast alignments. The Sh facies comprise fine- to coarse-grained, moderately to well sorted, angular to sub-angular sands. The Gmm facies form thick beds that can reach up to 40 cm. They include poorly sorted, granules to cobbles (2 mm–15 cm) and angular clasts. The Fl facies form fine, well-marked planar-based strata. The Y facies forms beds that are up to 3 m thick.

Distribution and stratigraphic relationship

This gravel unit is widely distributed, thereby forming most of the present-day landscape surface, not only for the studied area but also for the entire western slope of the Precordillera at this latitude (Fig. 3). It is a brown-yellow coloured, poorly consolidated, commonly gypsum cemented but occasionally carbonate cemented sedimentary succession in which the thicknesses progressively increase from the range piedmonts downstream. The thicknesses of this succession only reach several meters at the range piedmonts and progressively decrease to reach more than 100 m in the farther plains. Thus, a vertical cross-section of this succession roughly defines a wedge-shaped geometry that opens downslope from the ranges. The succession unconformably overlies all of the older stratigraphic units. To the east, it is directly deposited on an extensive bare rock surface and onlaps the range piedmonts (Fig. 3 and 6, profile AA′). In line with the change in the thicknesses, the proportion of the individual facies changes depending on the position in the landscape. Coarse-grained facies are dominant close to the ranges, whereas fine-grained facies are preponderant and Y facies are more frequent downslope. In both the Tesoro and Tesoro NE mine pit, this succession reaches *ca.* 80 m thick. In the Tesoro pit, it unconformably overlies the Tesoro III gravels and is composed by beds that dip *ca.* 5°W, whereas in the Tesoro NE pits the beds are dipping *ca.* 5°E.

CLAST COMPOSITIONS AND CLAST COUNTS

Clast counts were performed for 16 stations that are roughly homogenously distributed throughout a *ca.* 300 m thick stratigraphic column logged on the Atravesado gravels (Fig. 7, column A). Clast counts were also performed for 23 stations that are roughly homogenously distributed throughout the *ca.* 370 m thick stratigraphic column logged on the Tesoro II and III gravels and on the Arriero gravels at the Tesoro mine pit (Fig. 7, column B). One hundred clasts were counted inside a *ca.* 2 × 2 m square in each selected station. These clast counts were primarily carried out to identify lithologies that can be used to reconstruct the exhumation history of the porphyry Cu from the stratigraphic record. We paid special attention to the identification of the hypogene alteration mineralogy when performing the clast counts for two main reasons (Fig. 1). First, the hypogene mineralization zone has vertical extents of ≥2 km and presents a vertical mineralogical zoning pattern (e.g. Sillitoe, 2010). Consequently, the hypogene mineralogy can be used as relative indicator of the erosion level of a porphyry Cu. Second, the extent of the hypogene alteration (several square kilometres) is much greater than the size of the intrusive (diameters and lengths commonly of ≤1 km, respectively) that generate the porphyry Cu (e.g. Sillitoe, 2010). Therefore, it is more likely to find that this rock type constitutes a relatively large clast group. All of the clast lithologies can be linked to rock units from either the CMD and/or the immediate vicinity. Thus, the clast counts can additionally be used to perform a provenance study by comparing the clast lithology populations to the lithology of the rock units recognized in the 1:25.000 regional geological map of the district (Mpodozis & Cornejo, 2012; Antofagasta Minerals, unpublished) (Fig. 2).

The lithologies that compose the different clast groups can be divided into those that are indicative of a specific geological unit and those that are present in various geological units. Table 2 summarizes and classifies these lithologies. The α-β lava clast group is present within the entire stratigraphic record and is composed of aphanitic and porphyritic andesites and dacites. They constitute a clast group that represents between 25 and 60% (up to 100% in one case) of the clasts in the Atravesado and the Tesoro II gravels, between 10% and 35% of the clasts in the Tesoro III gravels, and between 35% and 45% of the clasts in the Arriero gravels. The fine-grained granitoids incorporate another clast group that is commonly recognized along almost all of the stratigraphic record. It is composed of medium- to fine-grained, equigranular and porphyric diorites and quarzodiorites. They make up a minor clast group (up to 25% of the clasts) in the Atravesado gravels, and is a large population along the entire stratigraphic column of the Tesoro pit: they represent between 20% and 50% of the clasts in the Tesoro II gravels, between 30% and 65% of the clasts in the Tesoro III gravels, and between 0–10% and 40% of the clasts in the Arriero gravels.

Two clast groups can be recognized as occurring only in the Atravesado gravels. One of these populations comprises the α-δ volcaniclastic clasts, which is made up of andesitic and dacitic tuffs and volcaniclastic sandstones and which commonly contain between 25 and 65% of the clasts but may include up to 85% of the clasts. Although silicified rock or residual quartz fragments, which commonly have limonite patinas and a vuggy appearance, occur in minor amounts (up to 25%), they are another distinctive clast lithology of the middle and upper part of the Atravesado gravels. These lithologies represent the advanced argillic hypogene alteration (labelled as A-altered in Table 2), which is formed by

Table 2. Clast groups determined from the clast counts performed in this work, including the clast lithology description and the geologic unit in which these lithologies can be found.

Label	Clast lithology description	Rock unit
α-δ lava	Brown, grey or slightly purple aphanitic and porphiric andesites and dacites, commonly with plagioclase, rarely with hornblende, quartz or pyroxene phenocrysts	Upper Cretaceous sedimentary and volcanic Quebrada Mala Formation and early Paleocene-early Eocene Cinchado Formation.
α-δ volcanoclastic	Andesitic and dacitic tuff and volcanoclastic sandstones	Upper Cretaceous sedimentary and volcanic Quebrada Mala Formation located on the western part of the studied area
Fine-grained granitoids	Equigranular medium to fine-grained diorites and quarzodiories and porphyric hornblende diorites and quarzodiorites, frequently with mafic crystals altered to chlorite and plagioclase altered to epidote	Early Cretaceous and Paleocene intrusions.
Poorly consolidated tuffs	Poorly consolidated light grey and white lapilli, ash and crystalline dacitic and rhyolitic tuffs with amphibole crystals	Mid-Upper Eocene sedimentary and volcanic rocks
ρ epizonal intrusion	Quartz and K-feldspar porphyric rhyolites	Epizonal Upper Cretaceous and Paleocene intrusions.
Coarse-grained granitoids	Coarse-grained granodiorites and granites	Upper Paleozoic basement
Conglomerates	Gypsum or carbonate cemented fine-grained conglomerates	Mid-Eocene-Mid-Miocene gravel deposits
A-altered	Undifferentiated silicified rock or residual quartz fragments commonly with limonite patinas and vuggy appearance	Advanced argillic hypogene alteration
S-altered	Altered porphyric rocks with abundant sericite and veins of quartz and boxworks	Sericitic hypogene alteration
P-altered	Green-grey and grey-brown-coloured clast, partially or totally altered to chlorite and epidote, with limonite and goethite and pyrolusite patinas	Propylitic hypogene alteration
Calcareous	Limestones and calcareous siltstones	Jurassic to Lower Cretaceous Caracoles Group

hydrothermal rock leaching at shallower levels (0–500 meters deep) on the roof of porphyry Cu deposits (e.g. Sillitoe, 2010; Fig. 1).

Several clast groups are observed only in the Tesoro II and III gravels and the Arriero gravels. One of these clast groups includes the poorly consolidated dacitic and rhyolitic tuffs (labelled as poorly consolidated tuffs in Table 2). They are present within the entire stratigraphic column of the Tesoro pit; they are almost absent in the Tesoro II gravels, they constitute a minor population of the clasts (5–10%) in the Tesoro III gravels, and can reach up to 25% of the clasts in the Arriero gravels.

The porphyric rhyolites clast (labelled as ρ epizonal intrusion in Table 2) constitutes a clast group restricted to the Tesoro III gravels, which constitutes between 5% and 20% of the clasts. One clast group that is mainly restricted to the Tesoro III gravels (10–30%) but which is also present in the Arriero gravels (10–15%), is made up of coarse-grained granodiorites and granites (labelled as coarse-grained granitiods in Table 2). The clasts of gypsum or carbonate cemented conglomerates (labelled as conglomerates in Table 2) are present in a proportion between 5 and 10% and are restricted to the Arriero gravels.

One key clast group includes the clasts showing propylitic hypogene alteration (P-altered in Table 1). This alteration type is formed by hydrothermal activity at relatively deep levels, below the advanced argillic hypogene alteration, in the marginal and upper parts of the porphyry Cu-related intrusion, between 500 and >2000 m deep (Sillitoe, 2010; Fig. 1). These clasts are present along the entire column of the Tesoro open pit (Fig. 7, column B) in lower proportions (5–10%); however, they appear in large proportions (15–50%) in the Tesoro II gravels. This alteration type comprises green-grey and grey-brown coloured clasts that are partially or totally altered to chlorite and epidote, with limonite and goethite and pyrolusite patinas. Another key clast group, concentrated in the Tesoro II gravels, around the lower exotic manto (25–50%), and in the limit between the upper part of the Tesoro III gravel unit and the lower part of the Arriero gravels (5–45%), contains altered porphyric rocks with abundant sericite and veins of quartz and boxworks. This lithology represents a sericitic hypogene alteration (S-altered in Table 2), which is related to hydrothermal activity at relatively deep levels, in the upper part of the porphyry Cu deposit between 500 and 1500 m deep (Sillitoe, 2010; Fig. 1).

Additional qualitative data with regard to the clast composition based on the sedimentary deposits studied in this work have been reported by Blanco & Tomlinson (2002) around the Tesoro and Tesoro NE mines (Fig. S1). These authors indicate that the main clast group in the Tesoro I gravels is composed of α-β lava clasts (55–90%); however, the A-altered clasts also represent an important clast group (10–40%). Another minor clast group corresponds to the fine-grained granitoids. In the Tesoro II gravels, these authors report two main clast groups: ρ clasts (40–70%) and coarse-grained granitoid clasts (30–60%). The prominent clast group (up to 50%) in the Tesoro II gravels is constituted by S-altered clasts. A minor clast group (10%) is formed by P-altered clasts. Another predominant clast group (40%) in this gravel unit corresponds to α-β lava clasts. Finally, two predominant lithologies are recognized in the Arriero gravels: α-β lava clasts (50%) and limestone and calcareous siltstone clasts (40%; labelled as calcareous in Table 2). Two minor clast groups (<5%) are made up of conglomerates and coarse-grained granitoid clasts, respectively.

GEOCHRONOLOGY

Dating efforts were concentrated on constraining the ages of the different gravel units as well as the age of the supergene mineralization in the CMD. Our main objective was to relate the supergene mineralization episodes with the timing of the deposition of the gravels. Age constraints are based on three U/Pb ages and one $^{40}Ar/^{39}Ar$ age from the interbedded tuff layers. Due to the lack of additional volcanic rocks suitable for a more detailed geochronology analysis, we also carried out U/Pb dating on eight detrital zircon samples to estimate the maximum depositional ages and complement the tuff eruption ages obtained from the volcanic layers. We also use these data to complement the provenance study. The sampling localities for both the tuff eruption and detrital zircon ages are shown in Fig. 3 and these ages are stratigraphically positioned on the columns given in Fig. 4. See Data S1 and S2 for details regarding the geochronology data.

Two types of supergene mineralization are identified in the CMD: (a) in-situ oxide (Esperanza, Esperanza Sur, Encuentro, Llano and Mirador) or leached cap zones (Cerro Coronado) overlaying hypogene porphyry Cu mineralization; (b) roughly tabular and stratigraphic controlled exotic Cu bodies, such as at El Tesoro and Tesoro NE (Mora *et al.*, 2004; Perelló *et al.*, 2010). Five $^{40}Ar/^{39}Ar$ ages and one new K-Ar in-situ supergene mineral age from the CMD are reported in this study. We also report one K-Ar supergene mineral age from the exotic Cu body at the Tesoro NE pit. The sampling localities for the supergene mineral ages are shown in Fig. 3 and the ages yielded from these samples are presented in Table 3a ($^{40}Ar/^{39}Ar$) and b (K-Ar).

$^{40}Ar/^{39}Ar$ and K-Ar geochronology

Volcanic tuff

One tuff deposit (Tuff1) directly overlying the Arriero gravels in the Mirador mine pit was sampled for $^{40}Ar/^{39}Ar$ dating in biotite (column 3 in Fig. 4). The analysis of this sample was done at the OSU Argon Geochonology Lab, CEOAS Oregon State University (USA). The sample shows a well-defined plateau age defined by at least three consecutive steps within analytical errors of 2σ and more than 58% of ^{39}Ar released gas. Thus, the 9.52 ± 0.02 Ma plateau age is considered as the age of the tuff eruption (Data S1).

Supergene mineralization

In-situ oxide zones are characterized by chrysocolla, atacamite and paratacamite, with lesser amounts of copper clays, copper wad and copper pitch (Cu-bearing manganese oxyhydrates) and minor amounts of copper-bearing phosphates (Perelló *et al.*, 2010). These minerals frequently occur together with supergene alunite group minerals (alunite, natroalunite, jarosite), which can be dated by the $^{40}Ar/^{39}Ar$ or K-Ar methods to determine the ages of the supergene mineralization (Vasconcelos, 1999).

Two $^{40}Ar/^{39}Ar$ ages for the supergene alunite were obtained from the samples collected at the Esperanza Sur (GMC-07-221) and Penacho Blanco (CM-12.4) porphyry copper, and three other $^{40}Ar/^{39}Ar$ ages from the jarosite sampled at the Esperanza Sur (GM-10-04 Jar 1) and Penacho Blanco (CM-12.5B and CM-12.5A) deposits (Fig. 2; Table 3a). Following the procedure proposed by Layer (2000) and Lanphere & Dalrymple (2000), the five samples were step-heated at increased laser power with a CO_2 laser beam at the SERNAGEOMIN $^{40}Ar/^{39}Ar$ Geochronology Laboratory (Chile) (detailed analytical procedures are given in Arancibia *et al.* (2006). Well-defined plateau ages were obtained by at least three consecutive steps within the analytical errors of 2σ and more than 58% of ^{39}Ar released gas. The isochron ages are generally indistinguishable from the plateau ages in all of the samples. Thus, the plateau ages are considered as being more reliable, except for sample GM-10-04 Jar 1 which shows a slight excess of atmospheric Ar detected in the isochron diagram, in which case the isochron age was considered instead. One additional K-Ar age for supergene alunite was obtained from a sample collected at the Cerro Coronado alteration zone (SGCM_183.2; Fig. 2). These data are complemented with one $^{40}Ar/^{39}Ar$ age and three K-Ar ages previously published by Perelló *et al.* (2010) and Sillitoe & McKee (1996) for the Esperanza Sur porphyry Cu. Thus, the ages of the in-situ supergene minerals yielded

from the Esperanza Sur are 25 ± 2 Ma, 22.9 ± 0.4 Ma, 21.2 ± 0.2 Ma, 20 ± 1 Ma, 15.1 ± 1.0 Ma and 12.6 ± 2.0 Ma, the ages of in-situ supergene minerals yielded from the Penacho Blanco are 22.0 ± 0.6 Ma, 14.1 ± 0.15 Ma and 12.8 ± 0.1 Ma, whereas the Cerro Coronado alteration zone yielded an age of 25.2 ± 0.8 Ma.

Exotic Cu mineralization mainly corresponds to chrysocolla with a smaller amount of copper wad and several Mn oxides and hydroxides (Campos *et al.*, 2015; Menzies *et al.*, 2015). Atacamite, paratacamite, malachite and azurite are also present as overgrowths patinas superimposed onto the primary copper minerals, or filling open spaces in the hosting coarse-grained sediments. The copper wad includes ramsdellite and cryptomelane, the latter of which is a mineral that can be dated with the $^{40}Ar/^{39}Ar$ or K-Ar methods (Vasconcelos, 1999). Exotic Cu mineralization is hosted by roughly tabular stratigraphically controlled bodies. Two exotic Cu bodies, hosted in the Tesoro II gravels and the Arriero gravels, respectively, can be recognized in the Tesoro pit (Fig. 8a). In the Tesoro NE pit, one exotic body is hosted by the Arriero gravels. In this manto, chrysocolla occurs as angular reworked clasts and as cement filling cavities and fractures, generating coatings around non-mineralized clasts in some cases. The copper wad forms cement following the sedimentary structures and is frequently truncated by overlying barren gravel beds (Fig. 8b). These textures indicate a syn-sedimentary origin for the exotic mineralization of the exotic-body hosted by the Arriero gravels in the Tesoro NE pit. A K-Ar age from cryptomelane sampled from the copper wad from this manto (TNE-AP) (Fig. 8c; Table 3b, column 4 in Fig. 4) yielded an age of 21.9 ± 1.2 Ma.

Zircon U/Pb Geochronology

Volcanic tuff

Three tuff layers interbedded in the Esperanza gravels were sampled for U/Pb zircon dating. U/Pb geochronological analyses were done at the Geochoronology Lab of the Massachusetts Institute of Technology (USA) (Data S1). All of the samples yielded U/Pb zircon ages with an uncertainty at the 2σ level of <1.5% for a set of 18–20 analyses, representing the best estimate for the age of the tuff deposition. Sample Car2 yielded an age of 42 ± 1 Ma and was sampled from a block and ash bed interbedded in the upper part of the Esperanza gravels at the Esperanza Sur area (column 1 in Fig. 4). Sample Car220 yielded an age of 43.05 ± 0.43 Ma and was sampled from the drill hole core TYC-162, *ca.* 220 m stratigraphically downward of sample Car2 (column 1 in Fig. 4). Finally, sample Bote-09-110 yielded an age of 44.7 ± 0.5 Ma and was sampled from drill core BTE_09, *ca.* 250 m below the surface (column 6 in Fig. 4).

U-Pb detrital zircon geochronology

Sand from fine-grained beds interbedded in the Esperanza, Atravesado I, Tesoro II and III and Arriero gravels was sampled for U/Pb detrital zircon dating. The geochronological analysis of four samples (BTE09, Car253, Car252 and Car257) was done at the Radiogenic Isotope and Geochronology Laboratory, Washington State University (USA) (Fig. 9). In an attempt to constrain the age of the upper and lower exotic Cu bodies at the Tesoro pit, four additional samples (AFMZr1,2,3, and Det0) were taken from the sand matrix of conglomerates from the stratigraphic column of the Tesoro open pit (column 5 in Fig. 4). The geochronological analysis of these samples was done at the Pacific Centre for Isotopic and Geochemical Research, at the University of British Columbia (Canada). The zircon population peaks and average ages were calculated using the Isoplot software (an add-in for Excel; Ludwing, 2008) and calculation of the maximum depositional ages was based on the procedures proposed by Gehrels (2010). For each sample, we consider the 10 younger zircons ages and use the TuffZirc routine of Isoplot to differentiate within these zircons ages the largest and youngest population (made of at least three zircon ages) for which the average age has a MSWD < 1. These populations correspond to the red boxes shown in the inset of each probability plot on Fig. 9. In the case of too-young zircons, for which the scatter from the younger population is not related to their uncertainty, Pb loss is suspected and these zircon ages are rejected. Too-old zircons that increase the MSWD over 1 are also rejected. Zircon ages that were not considered are shown by the blue boxes in the inset of each probability plot on Fig. 9. The maximum depositional ages correspond to the average obtained from the red boxes ages for each sample.

The Esperanza gravels. Sample Bote-09 yielded a dominant Carboniferous-Permian population ($n = 79$) that includes zircon ages between 270 and 319 Ma, with a most common value of 296 Ma; and a second Eocene population ($n = 19$) (43–48 Ma) with a peak at 45 Ma. Four ages (59, 61, 62 and 62 Ma) define a minor Paleocene population. The maximum depositional age of the hosting sediment is 44.6 ± 0.73 Ma, yielded from the average age of the youngest coherent group of nine zircons.

The Atravesado gravels. Two samples from this gravel unit show a wide distribution of zircon ages ranging almost continuously from the Paleocene to the late Eocene. Sample Car253 corresponds to a reworked tuff. In this sample, the zircon ages ($n = 44$) range between 37 and 70 Ma with three different populations in the relative probability plot: (1) a late Eocene (37–41 Ma) population ($n = 19$), with a peak at 39 Ma; (2) a mid-late Eocene (42–44 Ma)

Table 3. $^{40}Ar/^{39}Ar$ (A) and K–Ar (B) ages of supergene minerals from the Centinela district. The geochronology analyses on the supergene minerals were carried out at the Laboratorio de Geocronología of the Servicio Nacional de Geología y Minería (SERNAGEOMIN, Chile). The additional age constraints are from Sillitoe & McKee (1996) and Perelló *et al.* (2010).

Sample	Project/Prospect	Mineral	PlateauAge (Ma ± 2s)	Steps	% ^{39}Ar in plateau	Integrated Age (Ma ± 2s)	Isochron Age (Ma ± 2δ)	Steps	Intercept$^{40}Ar/^{39}Ar$ ± 2δ	Comments
(A) ^{40}Ar–^{39}Ar datin										
GM-10-04 Jar 1	Esperanza Sur	Jarosite	14.8 ± 0.5	6/9		14.8 ± 0.5	15.1 ± 1.0	6/8	294.8 ± 1.1	Sample with slight excess of argon, best estimation is the isochron age
GMC-07-221	Esperanza Sur	Supergene alunite	12.6 ± 2.0	8/8		13 ± 5	12.2 ± 2.4	8/8	295.6 ± 0.3	Well-defined plateau age. Sample with no excess argon
CM-12.4	Penacho Blanco	Supergene alunite	22.0 ± 0.6	4/7	58.3	17.5 ± 1.3	22.7 ± 1.6	4/7	293 ± 3	Well-defined plateau age. Sample with no excess argon
CM-12.5B	Penacho Blanco	Jarosite	14.1 ± 0.15	10/10	100	14.1 ± 0.6	14.05 ± 0.22	10/10	295.8 ± 0.9	Well-defined plateau age. Sample with no excess argon
CM-12.5A	Penacho Blanco	Jarosite	12.8 ± 0.1	5/8	88.1	12.8 ± 0.4	12.2 ± 0.6	5/8	290 ± 9	Well-defined plateau age. Sample with no excess argon
Perelló *et al.* (2010)	Esperanza Sur (ex-Telegrafo)	Supergene alunite	22.9 ± 0.4	4/8	64	21.49 ± 0.36	25 ± 2		284 ± 6	Supergene alunite from leached capping zone at Telégrafo

Sample	Project/Prospect	Mineral	K (%)	^{40}Ar ($\times 10^{-10}$ moles g^{-1})	$^{40}Ar/^{40}Ar$ total	Edad (Ma ± 2s)	Comments
(B) K-Ar dating							
SGCM_183.2[1]	Cerro Coronado	Supergene alunite	6.77	30 560	0.450	25.2 ± 0.8	Supergene alunite from the leached capping zone
TNE-AP[1]	Tesoro NE	Criptomelane	3.361	28 850		21.9 ± 1.2	Criptomelane in an exotic body of Cu in Tesoro NE
Sillitoe & McKee (1996)	Esperanza Sur (ex-Telegrafo)	Jarosite	2.55		10.4	20 ± 1	Jarositic leached capping
Perelló *et al.* (2010)	Esperanza Sur (ex-Telegrafo)	Supergene alunite	8.58	31 768	0.566	21.2 ± 0.2	Supergene alunite from the leached capping zone
Perelló *et al.* (2010)	Esperanza Sur (ex-Telegrafo)	Supergene alunite	9.54	31 961	0.824	19.2 ± 0.2	Supergene alunite from the leached capping zone

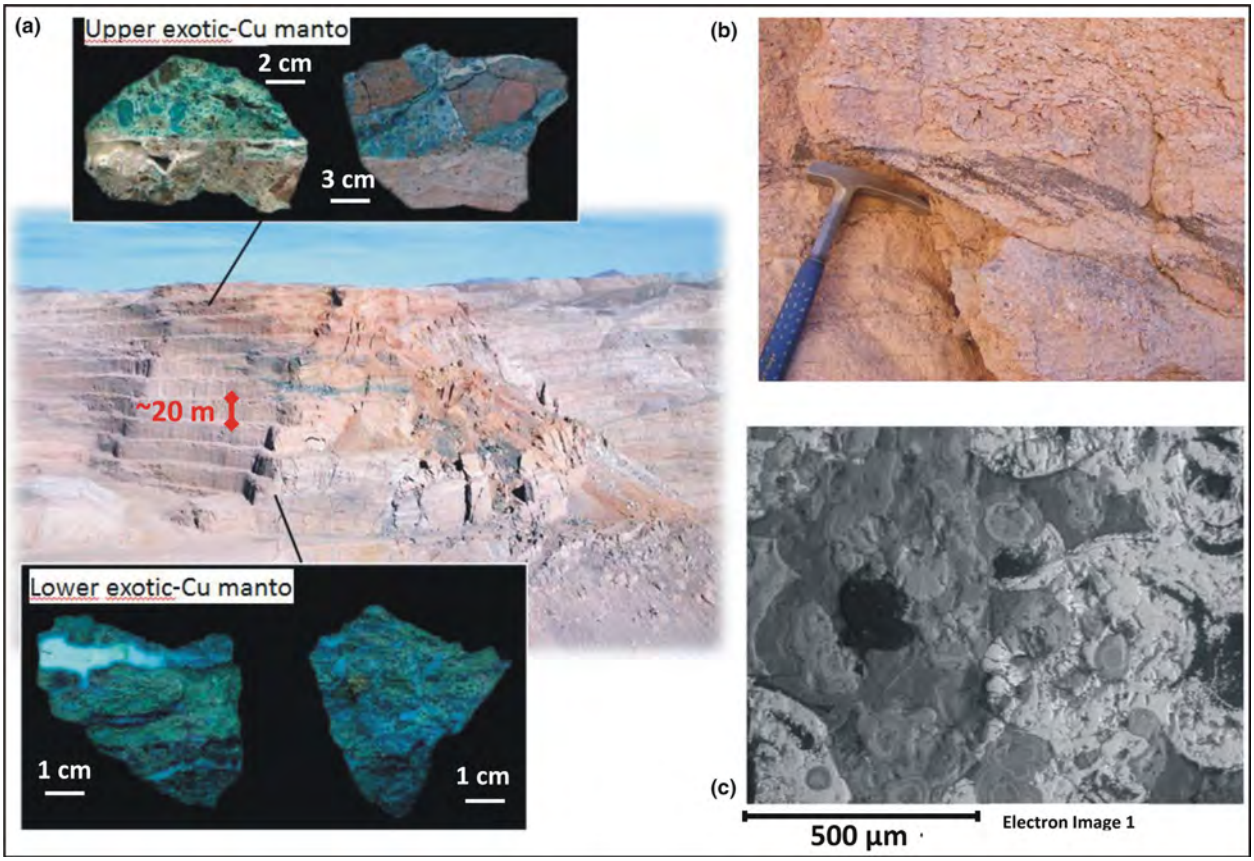

Fig. 8. (a) View of the El Tesoro open pit looking towards the southwest. The view shows the stratigraphic position of the lower and upper exotic Cu bodies. The characteristic textures of the exotic Cu mineralization in the lower and upper bodies are shown in the photographs below and over the open pit view, respectively. (b) Details of the syn-sedimentary textures shown by the copper-wad minerals exposed in the exotic Cu body at the Tesoro NE pit. (c) Scanning Electron Microscope image of the cryptomelane sampled for K-Ar dating.

population (n = 7), defining a peak at 43 Ma and (3) a late Paleocene (57–61 Ma) population (n = 14), showing a dominant value at 59 Ma. The average age yielded from the youngest coherent group of 8 zircons is 38.1 ± 0.36 Ma.

Sample Car252 shows zircon ages (n = 89) that are mainly concentrated between 39 and 70 Ma, with two large populations: one ranging between 39 and 46 Ma with a peak at 42 Ma (late Eocene, n = 76), and the other between 59 and 62 Ma with peak of 61 Ma (Paleocene, n = 5). An additional minor population (n = 4) in this sample has a mean age of 195 Ma (Sinemurian). The average age yielded from the youngest 10 zircons is 39.9 ± 0.42 Ma, which represents the maximum depositional age of the hosting sediment.

The Tesoro II gravels. Sample Car257 presents a dominant concentration of zircon ages defining a mid-late Eocene (39–46 Ma) population (n = 48) with peak at 42 Ma, a second large Paleocene (57–63 Ma) population (n = 11) at around 61 Ma, which is followed by a Late Cretaceous (68–74 Ma) population (n = 8) for which the most frequent value is around 71 Ma. The older zircon ages include two populations, a minor Jurassic (Sinemurian; 196–199 Ma) population (n = 4) with a peak around 196 Ma, and a large Carboniferous-Permian (274–309 Ma) population (n = 43) with a mean age of 292 Ma. The average age yielded from the youngest 10 zircons is 39.7 ± 0.78 Ma.

Sample AFMZr3 shows a large Eocene (35–49 Ma) population (n = 47) with a peak at around 43 Ma, followed by a Carboniferous-Permian (276–346 Ma) population (n = 35) with a mean age of 320 Ma. The maximum depositional age of the hosting sediment is 40.4 ± 1 Ma, yielded from the youngest coherent group of eight zircons.

The Tesoro III gravels. Sample Det0 presents the largest population (n = 55) of zircon ages related to the Carboniferous-Permian (266–339 Ma) with a peak around 299 Ma, followed by a second population (n = 16) with Late Cretaceous to Paleocene (58–75 Ma) ages which define two peaks, at 62 and 72 Ma, respectively. The maximum depositional age of the hosting sediment is 41.1 ± 1 Ma, yielded from the youngest coherent group of three zircons.

The Arriero gravels. Sample AFMZr2 yielded a large population (n = 88) of Carboniferous-Permian ages (284–342 Ma) centred at around 313 Ma. Only two zircons do not belong to this population and have younger late Eocene ages.

Finally, sample AFMZr1 contains a dominant population (n = 33) of late Eocene (36–43) zircon ages with a mean age of 39 Ma. In this late Eocene population, 10 individual zircon ages are younger than 39 Ma. A large Late Cretaceous-Paleocene population (n = 16) (58–70 Ma) with a peak at 64 Ma, followed by a large Carboniferous-Permian population (283–344 Ma) defining a peak at 329 Ma. The maximum depositional age of the hosting sediment is 37.6 ± 2.1 Ma, yielded from the youngest coherent group of nine zircons.

DISCUSSION

Timing of the sedimentation and supergene mineralization

Six gravel units with ages ranging between the mid-late Eocene and the mid-Miocene can be recognized in the CMD. The tuff eruption ages yielded from the interbedded tuff layers (45–42 Ma; Car2, Car220, BTE09-110) indicate that the deposition of the Esperanza gravels was nearly contemporaneous with the emplacement of most of the porphyry copper systems in the Centinela district (Fig. 10). On the other hand, the age for the base of the Arriero gravels is constrained by the *ca.* 22 Ma cryptomelane age (TNE-AP) yielded from the syn-sedimentary exotic Cu mineralization at the Tesoro NE open pit. It can consequently be considered as a minimum age for the base of this facies association. The minimum age for the Arriero gravels is constrained by the overlying volcanic ash that yielded 9.28 ± 0.05 Ma (SGCM_133.8, Fig. 10).

The late Eocene to Oligocene represents a magmatic and volcanic gap at the considered segment of the Central Andes (e.g. Stern, 2004; Kay *et al.*, 2005). Therefore, it is expected to find a gap in the maximum depositional age yielded from detrital zircon samples for this time span. Thus, the ages of the gravel units cannot be accurately constrained using the available detrital zircon geochronology data. In particular, the Tesoro II gravels are stratigraphically separated from the late Eocene Esperanza gravels by *ca.* 400 m of sediments that constitute the Tesoro I gravels. Thus, even if the Tesoro II gravels expose two late Eocene maximum depositional ages (*ca.* 40 Ma; Car257 and AFMZr3) intercalated at the base of the column at the Tesoro open pit, they may be much younger than *ca.* 40 Ma. On the other hand, the lowermost Atravesado gravels can be correlated to the Tesoro I gravels based on the sedimentary facies, clast compositions and stratigraphic position. Both the Tesoro I and the lowermost (*ca.* 200 m) Atravesado gravels are made up of the same facies which differ only in the proportion of coarse-grained facies vs. the fine-grained facies: that is, the Gcm and Gmm facies are dominant in the Tesoro I unit, whereas the Sm and Fsm dominates in the Atravesado unit. The Tesoro I gravels unconformably overlie the Esperanza gravels, whereas the Atravesado gravels can be recognized directly overlying the Esperanza gravels in the drill core BTE-09. Furthermore, the Tesoro I and the Atravesado gravels are the only gravel units along the Centinela stratigraphic record to include the distinctive population of clasts showing advanced argillic alteration. The Tesoro I and, at least, the lowermost *ca.* 200 m of the Atravesado gravels can be considered as lateral variations within the same stratigraphic unit (Fig. 10). On the other hand, both the Tesoro II and the uppermost *ca.* 100 m of the Atravesado gravels show an increase in the proportion of channelized stream flow deposits (Gpt and Spt facies) with respect to their respective underlying facies association. Thus, the Tesoro II and the uppermost Atravesado gravel deposits could be a lateral variation of the same stratigraphic unit.

The age yielded from in-situ supergene minerals ranges between 25.2 ± 0.8 at Cerro Coronado and 12.6 Ma at Esperanza Sur. These ages define a time span for the supergene processes in the Centinela district that roughly overlap the time span during which the Arriero gravels were deposited. However, based on these ages, we identify a gap in the supergene activity between *ca.* 19 Ma and *ca.* 15 Ma. Thus, the supergene ages can be grouped into two episodes, *ca.* 25–19 Ma and 15–12 Ma, which can be identified from all of the available ages as well as from individual oxide zones, for example as in the Esperanza Sur and Penacho Blanco areas (Table 2). The 21.9 ± 1.2 Ma K-Ar age yielded from cryptomelane at the Tesoro NE pit is part of the first *ca.* 25–19 Ma supergene age episode.

Sediment provenances and porphyry Cu unroofing

The porphyry copper systems were emplaced possibly >2 km under the surface at the same time during which the Esperanza gravels were deposited on the surface. Thus, the relevant mid-Eocene (43–48 Ma) detrital zircon population yielded from sample BTE09 (Fig. 9) can only represent the erosion products of the volcanic rocks deposited contemporaneously with these gravels (Fig. 11a). The other large detrital zircon population is the one represented by late Paleozoic zircons. The lack of Mesozoic and Paleocene detrital zircon age populations suggests that the Paleozoic population is directly related to the erosion of the late Paleozoic basement and not the result of recycled zircon. The late Paleozoic basement is nowadays exposed to the east (Sierra Agua Dulce) and north (Sierra Limón Verde) of the Centinela district (Fig. 2).

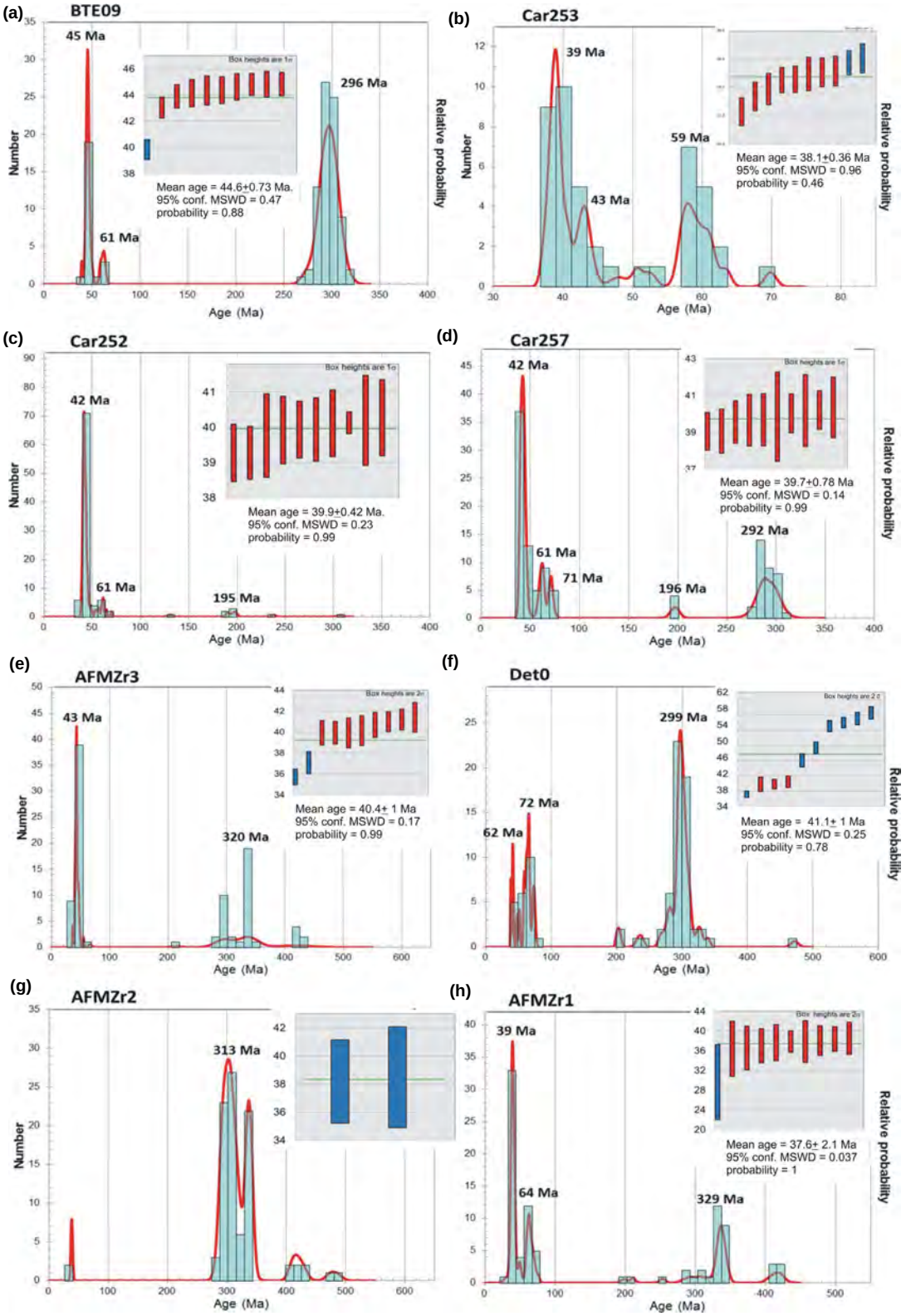

Fig. 9. Probability plots and maximum depositional ages (inset) of the detrital zircon population from samples taken from the CMD. Sample BTE-09 is sandstone from the BTE-09 drill core (column 6 in Fig. 4). Car253 (reworked tuff) and Car252 (sandstone) are samples from the Atravesado area (column 2 in Fig. 4). Sample Car257 is a sandstone bed from a drill core, taken 50 m below the base of the Tesoro open pit. See the text for explanation of the probability plots and insets.

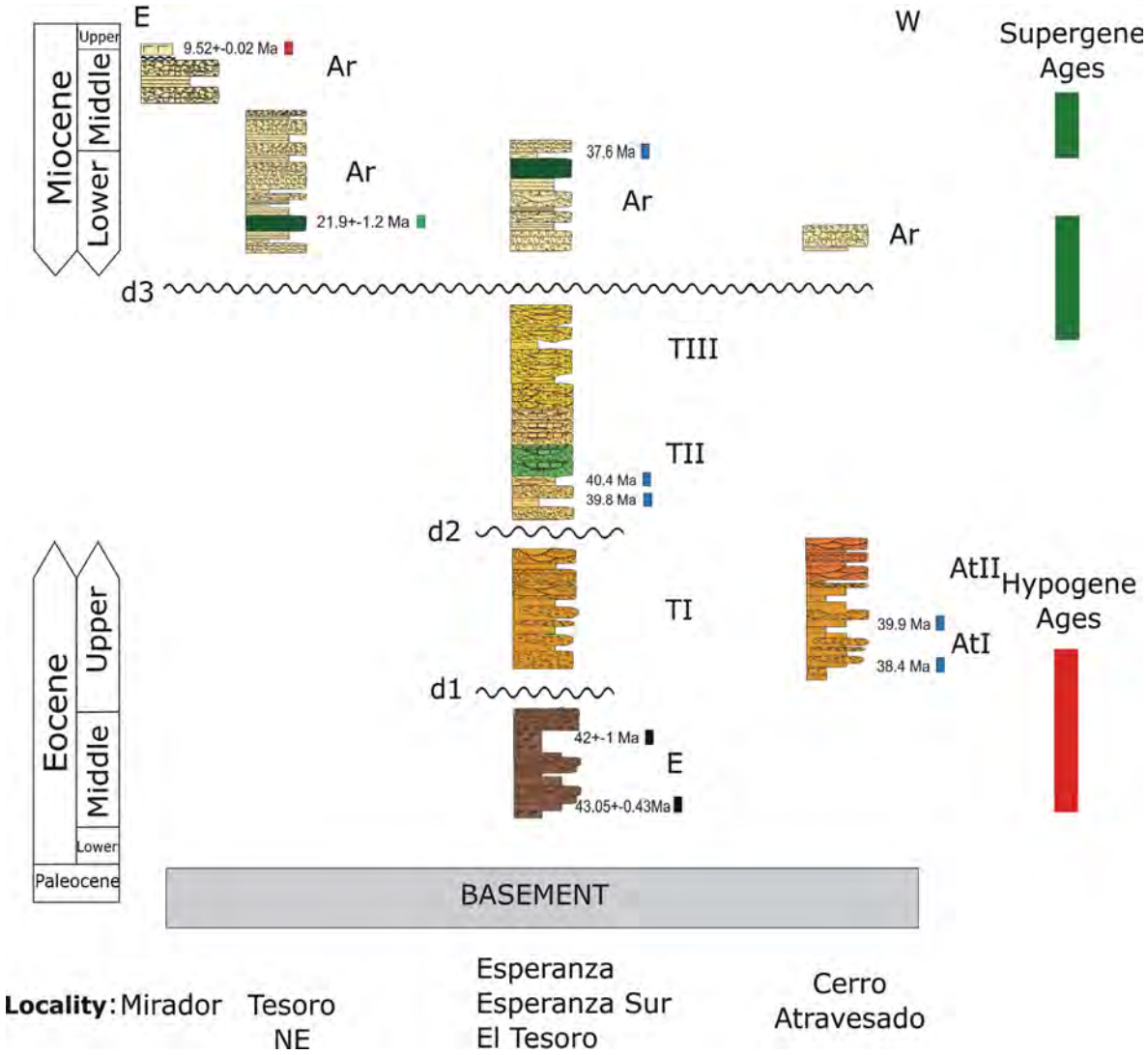

Fig. 10. Generalized stratigraphic columns arranged roughly along anEW direction including the reported geochronological data. The figure presents the stratigraphic contact and the stratigraphic relationships between the gravel units. The bars on the right side show the age ranges for hypogene (red) and supergene mineralization (green), as deduced from the hypogene ages reported by Perelló *et al.* (2010) and Mpodozis & Cornejo (2012) and the supergene ages presented in this work. The abbreviations and colours of gravel units are given in Fig. 3.

Two clast groups are present along the entire stratigraphic record from the Tesoro I gravels to the Arriero gravels. The α-β lava clasts frequently form outcrops of the Quebrada Mala Formation to the west of the studied area. Isolated outcrops of this formation are also recognized to the east covering the Jurassic-Early Cretaceous rocks. The α-β lava clast can also be recognized as composing the Paleocene Cinchado Formation, which currently outcrops to the south of the CMD (Fig. 2). Rock units that can be the source of the α-β clast are widely distributed in almost all directions in the CMD so these clasts cannot be used to infer sediment provenances. The fine-grained granitoids are a minor clast group in the Atravesado gravels and are an important population in the Tesoro II, III and Arriero gravels. These rock types can be only from the early Cretaceous and Paleocene intrusions that outcrop in the highest reliefs located to the east of the CMD.

A predominant clast group, exclusively recognized in the Atravesado gravels, corresponds to the α-δ volcanoclastic clasts. They are common rock types widely recognized along the Upper Cretaceous Quebrada Mala Formation and the Paleocene Cinchado Formation. On the other hand, the samples Car253 and Car254 show that the Atravesado gravels comprise two large detrital zircon populations, Paleocene and Eocene, respectively (Fig. 9). Although the Paleocene zircon populations (57–61 Ma, sample Car253 and 59–62 Ma, sample Car252) can be interpreted as recycled

Paleocene zircon sourced from younger Eocene rocks, the presence of the α–δ volcanoclastic clasts indicate that, at least part of the hosting sediment came from the erosion of Paleocene rocks. Therefore, the Paleocene zircon population can be related to the erosion of the Cinchado Formation. Furthermore, considering the wide distribution of the Quebrada Mala Formation throughout the CMD and immediate vicinity, the lack of a Late Cretaceous detrital zircon population suggests that this rock unit did not undergo erosion at that time and that the α–δ volcanoclastic clasts come exclusively from the erosion of the Paleocene rocks (Fig. 11b). The Cinchado Formation nowadays only outcrops at the highest reliefs located to the south of the CMD (Fig. 2). However, this formation probably extended to the north into the CMD at the time of the Atravesado I and II gravel depositions. Thus, in this area, the Cinchado Formation was eroded, contributing sediment to these gravel units.

A clast group included in the Tesoro I unit and the upper part of the Atravesado unit corresponds to the advanced argillic altered clasts. They indicate that hydrothermally altered rocks on the roof of a porphyry Cu, at shallower depths (0–500 m deep), underwent erosion. Moreover, these gravel units do not contain clasts showing hydrothermal alteration or hypogene mineralization, indicating the erosion of a porphyry Cu-related intrusions below the advanced argillic hypogene zones. This suggests that the Eocene detrital zircon populations in samples Car253 (37–44 Ma) and Car252 (39–46) result from the erosion of the mid-late Eocene volcanic rocks, such as those intercalated in the Esperanza gravels, and not from the erosion of the porphyry Cu-related intrusions, which were probably still buried during the accumulation of these gravels (Fig. 11b). The lack of Paleozoic detrital zircon populations and clasts from Paleozoic lithologies indicates either that sediment routing systems were not connected to the Paleozoic outcrops or that these rocks were protected from erosion by the cover of Paleocene and Eocene volcanic rocks.

The clast compositions of the Tesoro II and III gravels show a wider range of clast types, which include lithologies similar to most of the rock units currently outcropping in the CMD. The same conclusion can be reached from the U-Pb detrital geochronology data (samples Car257, AFMZr3 and Det0, Fig. 9), which show a wide range of ages and a greater number of detrital zircon populations than those recorded from the underlying gravel units, indicating that most of the rock units currently exposed at the CMD underwent erosion at the time of the deposition of these gravels.

In addition to the clast groups also recognized in the underlying gravel units, the Tesoro II and III gravels include poorly consolidated tuff clasts. This rock type is exclusive of the volcanic layers intercalated in the Esperanza gravels, which currently forms the Esperanza syncline and which are recognized as being interbedded in

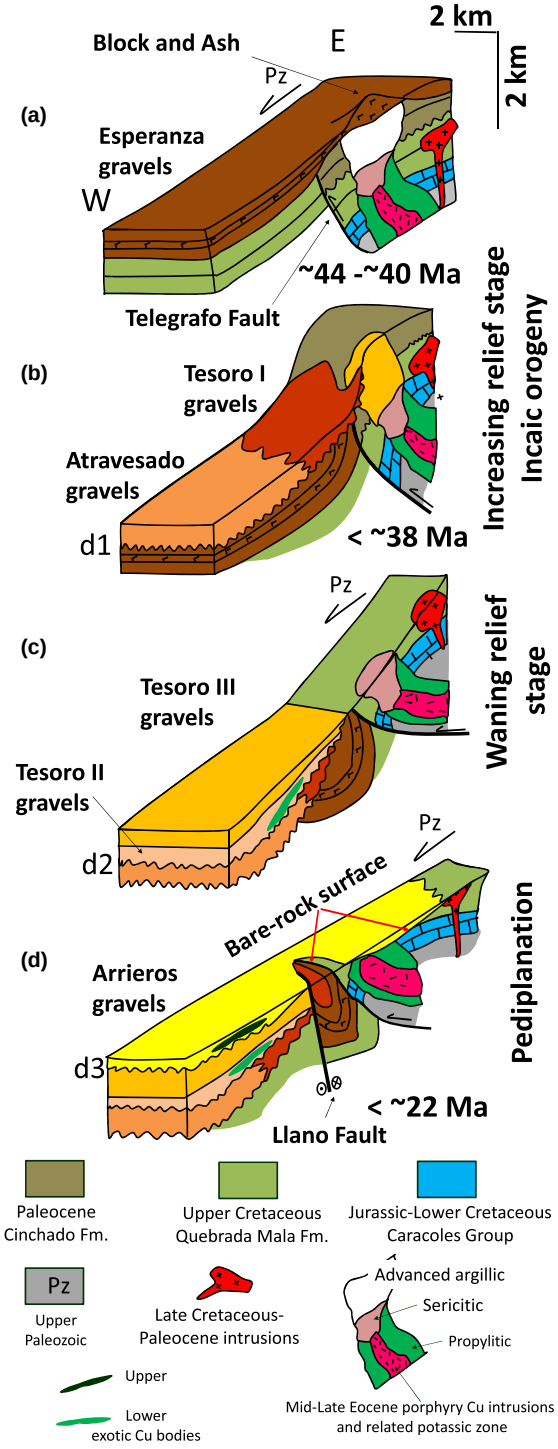

Fig. 11. Schematic depiction of the landscape evolution and related porphyry Cu unroofing sequence interpreted from the stratigraphy, geochronology and sedimentology data presented in this work. The approximate location of the section is that from the profile AA′ shown in Fig. 6. The horizontal and vertical scales are approximates. The dimensions of the porphyry Cu system are greatly overdone (compare with the profile AA′ in Fig. 6).

the BTE-09 drill core (Figs 3 and 11c). The clast types that are mainly restricted to the Tesoro III gravels, but which are also recognized in the Tesoro II gravels by Blanco & Tomlinson (2002), are the coarse-grained granitoids. This rock type can be recognized in the Upper Paleozoic basement that is currently exposed immediately to the north of the CMD and *ca.* 15 km to the east, in the Agua Dulce range (Fig. 2). The sediment sourced from the Upper Paleozoic basement to the Tesoro II and III gravels is also evidenced by the Carboniferous-Permian detrital zircon populations from samples Car257, AFMZr3 and Det0. A clast group restricted to the Tesoro III gravels, which contain between 5% and 20% of the clasts, is composed of a ρ-epizonal intrusion. This lithology can be recognized as constituting the epizonal Late Cretaceous and Paleocene intrusions (Fig. 11c).

The samples from the Tesoro II and III gravels show three large detrital zircon populations: Eocene (39–46 Ma, Car257; 36–49 Ma AFMZr3), Paleocene (57–63 Ma, Car257; peak at *ca.* 62 Ma, Det0) and Late Cretaceous (68–74 Ma, Car257; peak at *ca.* 72 Ma, Det0). As a result, the volcanic and intrusive lithologies that frequently constitute the Upper Cretaceous rock also constitute important clast groups in these gravels. It is interesting to note that most of the porphyry Cu deposits recognized immediately to the south of the Tesoro mine are hosted on Upper Cretaceous rocks from the Quebrada Mala Formation. The key clast groups correspond to the sericitic and propylitic altered clasts. Both alteration types are formed by hydrothermal activity below the advanced argillic hypogene zone, in the upper and marginal parts of a porphyry Cu, respectively, between 500 and 2000 m deep (Sillitoe, 2010). Hydrothermal sericite and alunite on the clasts included in the lower exotic Cu body at the Tesoro open pit have been dated by the Ar-Ar method yielding ages of *ca.* 40 Ma (Mora *et al.*, 2004; Perelló *et al.*, 2010), confirming that relatively deep parts of a late Eocene alteration zones related to a porphyry Cu underwent erosion and supplied sediments to the Tesoro II and III gravels. Moreover, the syn-sedimentary lower exotic Cu body hosted in the Tesoro II gravels indicates that copper-bearing minerals from a porphyry Cu are being oxidized and leached (Fig. 11c).

Similarly to the Tesoro II and III gravels, both clast lithologies and detrital zircon populations indicate that almost all of the rock units outcropping in the CMD were already exposed and eroded at the time of the Arriero gravel deposition. The conglomerate clasts are a distinctive population of this gravel unit that can only result from the erosion of the underlying gravel deposits. Another distinctive clast lithology contains limestones and calcareous siltstone rock fragments, a lithology that can be recognized in the Jurassic to Lower Cretaceous Caracoles Group and which forms the country rocks of some porphyry copper located to the east of the studied area (Figs 2 and 11d). The reworked Cu mineralized clasts in the upper exotic Cu body at the Tesoro open pit corroborate that the supergene mineralized deposits were exposed and eroded at the time when the deposition of the Arriero gravels was in progress.

Factors controlling the supergene and exotic copper mineralization

Geomorphology

The Incaic tectonic phase in northern Chile is an important episode of rock exhumation (exhumation rates from 100 to 200 m Ma^{-1}, Maksaev & Zentilli, 1999). This episode is inferred to have dominated the district during porphyry Cu development between 45 and 41 Ma (Perelló *et al.*, 2010). During this episode, the porphyry Cu deposits and their country rocks were upthrown to the west along the Telegrafo Fault over the Esperanza gravels (Mpodozis & Cornejo, 2012; Fig. 11a). From the timing and stratigraphy of the gravel units in the CMD, it can be deduced that the tectonic episode allowed for porphyry Cu exhumation over the last several million years through the deposition of the Esperanza and Tesoro II gravels (Fig. 11a–c). This tectonic episode was polyphasic, as evidenced by two angular unconformities: one separating the Tesoro I gravels from the underlying Esperanza gravels (d1 in Figs 10 and 11b) and the other one which separates the Tesoro II gravels from the underlying Tesoro I gravels (d2 in the Figs 10 and 11c). The polyphasic nature of the Incaíc orogeny has been widely documented (Reutter *et al.*, 1996; Tomlinson & Blanco, 1997a,b; Niemeyer & Urrutia, 2009; Dilles *et al.*, 2011). The d1 unconformity indicates that the Esperanza gravels were deformed prior to the Tesoro I gravel deposition. However, the Tesoro I and the correlative Atravesado gravels overlie the d1 unconformity and include advanced argillic altered clasts, which indicates that the shallow parts (0–500 m) on the roof of a porphyry Cu still underwent erosion by that time. Overlying the d2 unconformity, the exotic Cu body and the sericitic and prophylitic altered clasts indicate that a porphyry Cu underwent erosion only once the Tesoro II gravel deposition was in progress (Fig. 11c).

A tectonic episode that has a minor impact in terms of relief construction and exhumation, concerning the preceding tectonic history, is reflected in the d3 unconformity (Fig. 11d). On one hand, the clast and detrital zircon populations from the Arriero gravels are essentially similar to those of the immediately underlying gravel units, which indicate that the geological units that underwent erosion essentially have not changed. On the other hand, the upper part of the porphyry Cu-related intrusion is currently recognized close to the surface and already underwent erosion during the Tesoro II deposition. Thus, after this second tectonic episode, a minor amount

of unroofing occurred. Overlying the d3 unconformity, the Arriero unit forms a regionally extensive blanket of gravels, which has a vertical cross-section that roughly defines a wedge-shaped geometry that opens downslope from the range piedmonts. To the east, it is directly deposited on an extensive, smooth, low relief and gently sloping (<10°) bare rock surface and onlaps the range piedmonts (Figs 3 and 11c). According to Dohrenwend & Parsons (2009) and Strudley & Murray (2007), these geological features constitute a pediplain: the mountainous highlands and range piedmonts corresponding to the zone of erosion and denudation, the bare rock surface representing a transitional zone of lateral corrosion and sediment transport between the high and lowlands, and the Arriero gravels resulting from up-building by alluvium deposition in the zone of aggradation (Fig. 11c). The Arriero gravels can be interpreted as the result of landscape pediplanation (i.e. the landscape evolution that leads to the pediplain formation): the underlying bare rock surface continuously forming at the topographic front and subsequently being covered as the wanning of the relief and the retreat of this topographic front is going on. Considering the age constraints of the Arriero gravels, the CMD landscape already underwent pediplanation between the late Oligocene and the mid-Miocene, before the deposition of the 9.28 ± 0.05 Ma volcanic ash.

Late Oligocene to mid-Miocene landscape planation has also been reported in the Southern Atacama Desert (Clark *et al.*, 1967; Sillitoe *et al.*, 1968; Mortimer, 1973), the northernmost Chile (Mortimer, 1980; Bouzari & Clark, 2002) and southern Peru (Quang *et al.*, 2005). In the southern Atacama Desert (26–28°, Lat.S), *ca.* 500 km north of the CMD, the Atacama Gravels deposited during this time span by alluvial fan backfilling as the piedmonts and the valley sides retreated to form the Atacama Pediplain (Mortimer, 1973; Riquelme *et al.*, 2003, 2007; Bissig & Riquelme, 2009). Similarly to what is observed at the CMD, pediplanation had ceased before the late Miocene, as indicated by a *ca.* 10 Ma ignimbrite that covers the Atacama Pediplain (Clark *et al.*, 1967; Cornejo *et al.*, 1993; Riquelme *et al.*, 2007). Likewise, the flat surfaces that compose the forearc region of northernmost Chile, between the Arica and Iquique latitude (18–20°, Lat.S), were largely formed in the mid-Miocene, before the entrenchment of the present-day canyons at *ca.* 10 Ma (e.g. Farías *et al.*, 2005; Garcia *et al.*, 2011). Landscape pediplanation seems to be a generalized geomorphic process to most of the Precordillera and Central Depression of the Atacama Desert of northern Chile and southern Peru, which operated in the course of the late Oligocene to the mid-Miocene times, upon which the landscape has not been essentially modified.

Porphyry Cu deposits are emplaced at a depth of about 2 km and their exposure at the surface can be used to track landscape exhumation (Yanites & Kesler, 2015). The geochronology data along with the clast lithology and the detrital zircon populations recorded by the gravel units of the CMD provide a useful depth-time marker of the crustal level that underwent erosion during porphyry Cu exhumation. Regardless of the particularities in the tectonic evolution, such as the polyphasic nature of the main tectonic episodes and the existence of a subsequent minor tectonic episode, the gravel units of the CMD record an entire geomorphologic cycle that includes and follows the Incaic orogeny (Fig. 1). The gravel units that underlie the d2 angular unconformity represent an important erosion and rock exhumation event that can be related to the increasing and subsequent waning relief stages of the landscape evolution (Fig. 11b,c). In the course of this time span, between 500 and 2000 meters of rocks were unroofed and the porphyry Cu intrusions were driven up close to the surface where it could be weathered and oxidized. The subsequent geomorphological evolution is recorded from the Tesoro II gravels onward and occurs without major unroofing. This stage of the landscape evolution can be related to pediplanation (Fig. 11d). The geomorphologic cycle deduced from the gravel units is also seen from thermal modelling of low temperature thermochronology data (Sanchez *et al.*, 2015). The porphyry Cu deposits in the CMD underwent a relatively rapid cooling since their emplacement at *ca.* 45–41 Ma until *ca.* 30 Ma that can be associated with the increasing stage of landscape evolution. After 30 Ma, the porphyries underwent a relatively slow cooling related to low exhumation rates, which represents the early waning relief stage of landscape evolution and the subsequent landscape pediplanation (Sanchez *et al.*, 2015). Thus, a time shift between the main post-Incaic exhumation and the supergene copper mineralization episodes of the order of 10–20 Ma can be deduced from the thermochronology data (Olivares, 2001; Sanchez *et al.*, 2015) and the supergene mineralization ages presented herein. This time shift agrees with that proposed in a review of all the thermochronology and supergene age data performed in Northern Chile (Arancibia *et al.*, 2006).

Geobarometry and geochronology data along with geochemical mass balances yielded from La Escondida porphyry Cu, also located in the Antofagasta region, suggest that *ca.* 3000 m of rocks were eroded between *ca.* 33 Ma and *ca.* 18 Ma (Alpers & Brimhall, 1988). The porphyry Cu exhumation began with the erosion of the shallow advanced argillic alteration and ended with the erosion of the deep sericitic and prophylitic alteration. This erosion sequence through the time, for the vertical zoning pattern of the hypogene mineralization, is similar to that deduced from the clast composition of the gravel units in the CMD. From the Tesoro I through the Tesoro II, the

gravel deposits of the CMD record the exhumation history of one or several mid- to late Eocene porphyry Cu deposits, located to the east of these gravels, from the depths of emplacement to position near surface, a depth at which they can be found nowadays. Similarly, after the erosion of the sericitic and prophylitic alteration zone and the beginning of supergene mineralization at *ca*. 18 Ma, the Escondida porphyry Cu remains close to the surface up to the present day (Alpers & Brimhall, 1988). In the CMD, the age distribution from the in-situ and exotic supergene minerals (*ca*. 25–12 Ma) concentrate in the time span during which the landscape underwent pediplanation and the Arriero gravels deposited. The lower exotic Cu body hosted in the Tesoro II gravels indicates that supergene mineralization occurred during the waning relief stage of the landscape evolution or relatively early during the pediplanation stage. The corresponding in-situ supergene mineralization has not been recognized because it was probably subsequently eroded.

The role of landscape peneplanation (a broader term used to define any extensive low-relief erosional surface, including the pediplains e.g. Phillips, 2002) on the formation and distribution of world-class supergene metalliferous ore deposits has been widely reported. Certainly, ancient flat landsurfaces that remained almost immune to erosion for tens of millions of years account for the widespread distribution of world-class supergene iron, manganese and aluminium ore bodies as those exposed in the southeastern Brazil, or those in the Western Australia (e.g. de Oliveira Carmo & Vasconcelos, 2006; Spier *et al.*, 2006). At Malawi, Southeast Africa, Cenozoic landscape peneplanation allowed strong chemical weathering and erosion and favoured the formation of supergene mineral deposits enriched in aluminium (Dill, 2007). In several places of the world including USA, Canada, Sweden, Iran and West Africa, diverse metalliferous deposits (copper, silver, iron, nickel, uranium, gold and REE deposits) are associated with the extensively developed sub-Cambrian surface. Many of these deposits show evidence of intense weathering that is controlled by the widespread sub-Cambrian peneplanation (Parnel *et al.*, 2014). Supergene alteration and enrichment due to oxidation not only upgrade the value of the ores, but also generate an unprecedented flushing of metals to the chemistry of the earliest Cambrian ocean, which in turn would contributed to the marked early Cambrian faunal evolution (Parnel *et al.*, 2014).

In the Atacama Desert, the relationship between pediplains and supergene activity has been investigated from the pioneer works of Clark *et al.* (1967), Sillitoe *et al.* (1968) and Mortimer (1973). In the southern Atacama Desert, the widespread supergene activity observed during the late Oligocene and early Miocene (Mote *et al.*, 2001) roughly coincides with available age constraints on the formation of the Sierra Checos del Cobre pediplain (Mortimer, 1973). Similarly, the middle Miocene exotic copper mineralization coincides with the initial stages of the formation of the Atacama pediplain (Mote *et al.*, 2001; Riquelme *et al.*, 2007; Bissig & Riquelme, 2010). Successive episodes of renewed uplift and pediplanation are responsible of the formation of a thick (up to 450 meters depth) weathering profile at Cerro Colorado mine, in the Precordillera of northernmost Chile (Bouzari & Clark, 2002). Although these authors relate the reactivation of intense leaching to drastic fall in the water table, which would be triggered by regional uplift, no precise geochronologic constraints on the pediplains are available that allow correctly associate these landforms features to the supergene episodes. A similar statement can be postulated in the Cordillera Occidental of southern Peru. In this region, the large-scale landscape is composed of remnant pediplain surfaces disposed at different elevations. Supergene mineral ages indicate two main supergene episodes responsible of the upgrading of some ore deposits. Late Eocene supergene profiles beneath highest pediplains would result from a first episode of regional uplift and landscape entrenchment, whereas late Oligocene to early Miocene supergene profiles beneath lowest pediplains would result from renewed uplift and landscape entrenchment episode (Quang *et al.*, 2005). In general, supergene ages are used to constraint the age of the pediplains and no direct geochronologic data are available allowing to determine if supergene profile result from landscape entrenchment or from the pediplain formation. Our data shed light on this issue. The Arriero gravel deposition is clearly related to pediplain formation and evolution, and the timing in which these gravels are deposited roughly overlap the time span in which supergene mineralization took place. No landscape entrenchment can be invoked to explain the supergene age distribution across the CMD. On-going pediplanation during the Arriero gravels deposition did not only favour supergene mineralization, but also preserved the former supergene mineralized zones from significant erosion. Supergene enrichment of metalliferous ores is clearly expected to occur in landscapes that remain relatively stable for millions of years under prevailing warm and wet climatic conditions. Similarly, pediplanation can represent a geomorphologic condition favourable for protracted supergene activity in arid to semi-arid climates as those prevailing during the late Cenozoic in the Atacama Desert.

Paleoclimate

Paleoclimate apparently plays an important role in the operation of supergene processes (e.g. Clark *et al.*, 1990; Chávez, 2000; Hartley & Rice, 2005; Arancibia *et al.*, 2006; Vasconcelos *et al.*, 2015). The age distribution yielded from in-situ and exotic supergene minerals

indicate that supergene processes in the CMD were active between late Oligocene and mid-Miocene, mainly during the early Miocene, a time span that concentrates most of the supergene ages in northern Chile. Considering that supergene environments require enough groundwater to promote oxidation and leaching of hypogene sulphides (e.g. Vasconcelos, 1999; Chávez, 2000), then this time span must have been, at the very least, a time with prevailing semi-arid climate conditions (i.e. >100 mm $year^{-1}$, Clark *et al.*, 1990). It is interesting to note that the early Miocene has been also considered as a time of warm and humid climate conditions elsewhere in the southern hemisphere. Paleoflora records indicate that warm and humid climate condition prevailed in the Central Chile and Argentina at that time (Hinojosa, 2005; Hinojosa & Villagran, 2005). Comprehensive geochronological studies that consider the distribution of supergene Mn ages in weathering profiles from the central Queensland, Australia, indicate warm and humid conditions during the early Miocene (Li & Vasconcelos, 2002). Additional evidence for wet and relatively warm climates over much of Australia during the first part of the Miocene comes also from micro-facies analysis of carbonate sediments, paleosols clay mineralogy and the palaeontologic record (Truswell, 1993; Brachert & Dullo, 2000). On the other hand, paleoclimate records, which indicate the onset of cold and arid conditions at the mid-Miocene, are thought to be of global significance as it coincides with a major growth of the east Antarctic ice sheet (Li & Vasconcelos, 2002; Flower & Kennett, 1994; Zachos *et al.*, 2001). Furthermore, the onset of the hyperarid conditions in the Atacama Desert since mid-Miocene it is widely accepted (e.g. Sillitoe & McKee, 1996; Dunai *et al.*, 2005; Rech *et al.*, 2006, 2010; Evenstar *et al.*, 2009; Jordan *et al.*, 2014 Oerter *et al.*, 2016). It is also interesting to note that two major peaks, at 20.2 Ma and 16.5 Ma, can be deduced from the distribution of supergene Mn ages in weathering profiles from the central Queensland (Li & Vasconcelos, 2002).

The supergene minerals ages in the CMD define two supergene episodes, at 25–19 and 15–12 Ma, which overlap with the *ca.* 20 and *ca.* 14 Ma episodes of intense supergene activity that have been postulated for the Atacama Desert (e.g. Sillitoe & McKee, 1996; Arancibia *et al.*, 2006). In the CMD, these two supergene episodes are not related to unroofing episodes as has been previously proposed elsewhere in the Atacama Desert (e.g. Bouzari & Clark, 2002; Quang *et al.*, 2003; Hartley & Rice, 2005; Sillitoe, 2005). They rather result from early Miocene climate conditions in which relatively wet, weathering-prone conditions, alternate with relatively dry, erosion-prone conditions as it has been proposed to explain the major peaks in the distribution of supergene Mn ages from the central Queensland (Li & Vasconcelos, 2002).

Climate vs erosion vs time

Although pediplanation was a necessary condition to significantly enrich the copper by supergene processes in the Centinela district, we do not claim that pediplanation is a necessary condition in all of the other situations. For example, in uplifted and dissected Andean regions such as those in the Salvador, El Hueso and La Coya regions (Mote *et al.*, 2001; Bissig & Riquelme, 2009, 2010), the descent of the water table driven by incipient river incision may better explain the formation of thick Oligocene and late Miocene supergene mineralization profiles on ore deposits. These examples have been subjected to orographic rainfall and thus correspond to another climatic context. Likewise, other geomorphologic conditions must be considered to explain the thick supergene profiles formed in Pliocene porphyry Cu belts under climatic regimes of higher precipitation such as those of Papua New Guinea and Philippines (e.g. Sillitoe, 2005). The deepest known oxidation profiles (600 m thick) recognized in the Surigao district, Philippines, surely are not possible to develop under climate conditions other than those highly rainy that prevailed during the very rapid uplift and exhumation of the porphyry Cu (Braxton *et al.*, 2012). In prolonged arid areas such as the CMD, low erosion rates during pediplanation may constitute a necessary condition for the supergene enrichment of copper, as it has already been suggested by Sillitoe (2005). The appropriate balance between erosion rate and water table descent rate that allowed the development of the weathering profile seems to be promoted by a landscape evolution characterized by pediplanation. However, such a favouring geomorphologic condition also requires the prevalence of a relatively wetter climate condition (semi-arid with respect to the arid to hyperarid climatic condition prevailing in the late Cenozoic history of the Atacama Desert) to efficiently allow the supergene mineralization processes to occur. Both landscape pediplanation and semi-arid climate conditions took place during the early Miocene on the Atacama Desert.

On the other hand, time is another important factor in the development of thick supergene profiles as emphasized by Sillitoe (2005). However, the time required to form mature supergene profiles most likely depends on the balance between exhumation and precipitation rates. Thus, for example, the Surigao porphyry Cu district, in Papua New Guinea, was leached and enriched since emplacement below sea level only in the last 2.3–2.1 Ma (Braxton *et al.*, 2012). In this case, high exhumation rates (2.5 km Ma^{-1}) are balanced by high precipitation rates (2000–4000 mm $year^{-1}$) allowing the formation of a mature supergene profile (600 m thick) in a time span lasting for not more than few hundred thousand years (Sillitoe, 2005). In contrast, when primary ore deposits

are subjected to low exhumation rates (50 m Ma^{-1} in the Precordillera of the Atacama Desert, Maksaev & Zentilli, 1999) and low precipitation rates (e.g. 100 mm $year^{-1}$ in arid climate), the formation of mature supergene profiles may require more than 10 Ma (between *ca.* 25 and 12 Ma) as is suggested by the supergene mineralization ages of the CMD.

Implications for exploration

In recent years, exploration for copper resources around the world has shown an increasing interest for supergene-enriched deposits buried beneath piedmont gravels developed on arid to hyperarid environments, similar to those herein defined as the Arriero gravels. Traditionally, geochemical and geophysical tools have been used to locate buried ore deposits through exploration campaigns that are commonly characterized by a high investment cost and high degree of uncertainty of success. One of the main weakness of today's exploration programmes on areas covered by gravel deposits is that they do not take into consideration the long-term large-scale landscape evolution and the depositional history of the cover gravels. We propose that the integration of geomorphological and sedimentological data with provenances studies is a powerful tool to better define prospective targets, increasing the efficiency of exploration programmes that are looking for porphyry Cu deposits covered by gravels which are developed on arid to hyperarid environments.

CONCLUSION

Seven gravel units with ages ranging between the mid-late Eocene to the mid-Miocene can be recognized in the CMD. The geochronology data along with the clast lithology and the detrital zircon populations provide a useful depth-time marker that can be used to reconstruct an unroofing history for the porphyry Cu located immediately to the east of the studied gravel outcrops. This unroofing history combined with the distribution and the stratigraphic relationships between the gravel units and gravel substratum rocks can be used to interpret the landscape evolution of the CMD as the result of a geomorphological cycle that ranges from the increasing stage through the declining stage of landscape evolution, including the latest pediplanation stage, and which is triggered in the mid-late Eocene by the Incaic orogeny. The older gravel units are the Esperanza gravels that were deposited nearly contemporaneously with the emplacement of most of the porphyry copper systems. The subsequent Tesoro I to Tesoro II gravels record the unroofing of the porphyry Cu, from the advanced argillic zone to the sericitic and prophylitic hypogene zones. The porphyry Cu intrusions were exhumed sometime between the late Eocene and the Oligocene and remain close to the surface up to the present day. After a minor tectonic episode, which has virtually no impact on the porphyry Cu unroofing, the Arriero gravels deposited and the landscape continues to evolve by pediplanation. The supergene mineral ages of the CMD define a time span (*ca.* 25–12 Ma) for the supergene processes that roughly overlap the time span during which the Arriero gravels deposited. We propose that pediplanation favours supergene mineralization and also helped preserve the former supergene mineralized zones from significant erosion. Such a favourable geomorphologic condition also requires a relatively wetter (semi-arid, >100 mm $year^{-1}$) climate condition to efficiently allow the supergene processes to occur. Low erosion rates during pediplanation may constitute a necessary requirement for the effectiveness of the supergene processes in such climatic conditions. Furthermore, most of the supergene ages are concentrated in the early Miocene, a time on which the global prevailing climate was apparently warm and humid. The supergene ages can be grouped into two episodes, *ca.* 25–19 Ma and 15–12 Ma, which overlap with the *ca.* 20 and *ca.* 14 Ma episodes of intense supergene activity that have been postulated for the Atacama Desert. In the CMD, these two supergene age episodes are not related to unroofing episodes. Therefore, the gap between 19 and 15 Ma in the supergene mineral ages can be related to a drier climatic episode which limited the supergene processes, as occurred with the onset of hyperaridity climatic condition after the mid-Miocene. Finally, the combined use of data and observations as done on this paper can be very useful on planning exploration campaigns for porphyry Cu deposits that are cover by gravels in desert environments, such as the northern Chile, southern Peru, southwest USA and Mongolia.

ACKNOWLEDGEMENTS

The present study was funded by FONDECYT Project No. 1121041, Antofagasta Minerals S.A. and the LMI-COPEDIM project (IRD, France). We gratefully acknowledge Adrian Hartley and an anonymous reviewer for their useful reviews which largely improved this work.

SUPPORTING INFORMATION

Additional Supporting Information may be found in the online version of this article:

Table S1. Table of equivalences between the stratigraphic units previously defined in the Centinela district and the gravel units presented in this work.

Fig. S1. Geologic map reported by Blanco & Tomlinson (2002). The focus is on the gravel units exposed

around the Tesoro and Tesoro NE mine and includes the qualitative data for the clast composition from these gravels. The equivalence between these gravels units and the gravel units reported in this work is presented in the Table S1.

Data S1. Volcanic tuff age geochronological data.

Data S2. Detrital Zircon geochronological data.

REFERENCES

Aguilar, G., Riquelme, R., Martinod, J., Darrozes, J. & Maire, E. (2011) Erosion rates variability on landscape's transience state in the semiarid Chilean Andes. *Earth Surface Processes and Landforms*, **36**, 1736–1748.

Alpers, C.N. & Brimhall, G.H. (1988) Middle Miocene climatic change in the Atacama Desert, northern Chile: evidence from supergene mineralization at La Escondida. *Geol. Soc. Am. Bull.*, **100**, 1640–1656.

Amundson, R., Dietrich, W., Bellugi, D., Ewing, S., Nishiizumi, K., Chong, G., Owen, J., Finkel, R., Heimsath, A., Stewart, B. & Caffee, M. (2012) Geomorphologic evidence for the late Pliocene onset of hyperaridity in the Atacama Desert. *Geol. Soc. Am. Bull.*, **124**, 1048–1070.

Anderson, J. (1982) Characteristics of leached capping and techniques of appraisal. In: *Advances in the Geology of the Porphyry Copper Deposits* (Ed. by S.R. Titley), pp. 275–296. University of Arizona Press, Tucson, AZ.

Arancibia, G., Matthews, S.J. & de Arce, C.P. (2006) K–Ar and $^{40}Ar/^{39}Ar$ geochronology of supergene processes in the Atacama Desert, Northern Chile: tectonic and climatic relations. *J. Geol. Soc. London*, **163**, 107–118.

Arriagada, C., Roperch, P., Mpodozis, C. & Cobbold, P.R. (2008) Paleogene building of the Bolivian orocline: tectonic restoration of the Central Andes in 2-D map view. *Tectonics*, **27**, TC6014, 14 p. https://doi.org/10.1029/2008TC002269.

Basso, M. & Mpodozis, C. (2012) Carta Cerro Quimal, Región de Antofagasta. Servicio Nacional de Geología y Minería, Carta Geológica de Chile, Serie Geología Básica, 143, 1-46. 1 mapa escala 1:100.000. Santiago, Chile.

Bissig, T. & Riquelme, R. (2009) Contrasting landscape evolution and development of supergene enrichment in the El Salvador porphyry Cu and Potrerillos-El Hueso Cu–Au districts, Northern Chile. In: *Supergene Environments, Processes and Products* (Ed. by Titley S.) *Soc. Econ. Geol. Spec. Publ.*, **14**, 59–68.

Bissig, T. & Riquelme, R. (2010) Andean uplift and climate evolution in the southern Atacama Desert deduced from geomorphology and supergene alunite-group minerals. *Earth Planet. Sci. Lett.*, **299**, 447–457.

Blanco, N. & Tomlinson, A. (2002) Estudio estratigráfico y sedimentológico del Distrito Minero El Tesoro. Unpublished report, 29 pp.

Bordy, E.M. & Catuneanu, O. (2001) Sedimentology of the upper Karoo fluvial strata in the Tuli Basin. *J. Afr. Earth Sci.*, **33**, 605–629.

Bouzari, F. & Clark, A. (2002) Anatomy, evolution, and metallogenic significance of the supergene orebody of the Cerro Colorado porphyry copper deposit, I Región, Northern Chile. *Econ. Geol.*, **97**, 1701–1740.

Brachert, T.C. & Dullo, W.C. (2000) Shallow burial diagenesis of skeletal carbonates; selective loss of aragonite shell material (Miocene to Recent, Queensland Plateau and Queensland Trough, NE Australia); implications for shallow coolwater carbonates. *Sediment. Geol.*, **136**, 169–187.

Braxton, D.P., Cooke, D.R., Dunlap, J., Norman, M., Reiners, P., Stein, H. & Waters, P. (2012) From crucible to graben in 2.3 Ma: a high-resolution geochronological study of porphyry life cycles, Boyongan-Bayugo copper-gold deposits, Philippines. *Geology*, **40**, 471–474.

Brimhall, G.H., Alpers, C.N. & Cunningham, A.B. (1985) Analysis of supergene ore-forming processes and ground water solute transport using mass balance principles. *Econ. Geol.*, **80**, 1227–1256.

Campos, E., Menzies, A., Sola, S., Hernández, V., Riquelme, R. & Barraza, M. (2015) Understanding Exotic-Cu Mineralisation: Part I – Characterization of Chrysocolla. 13th SGA Biennial Meeting, France.

Carretier, S., Tolorza, V., Rodriguez, M.P., Aguilar, G., Martinod, J., Riquelme, R., Christophoul, F., Charrier, R., Gayer, E., Farías, M., Audin, L. & Lagane, C. (2014) Erosion in the Andes between 27S and 40S: Tectonic, climatic or geomorphic control ?. In: *Geodynamic Processes in the Andes of Central Chile and Argentina* (Ed. by Sepúlveda S.A., Giambiagi L.B., Moreiras S.M., Pinto L., Tunik M., Hoke G.D. & Farías M.) *Geol. Soc. London Spec. Publ.*, **399**. https://doi.org/10.1144/sp399.16.

Chávez, W.X. (2000) Supergene oxidation of copper deposits: zoning and distribution of copper oxide minerals. *Soc. Econ. Geol. Newsletter*, **41**, 1–21.

Clark, A.H., Mortimer, C. & Sillitoe, R.H. (1967) Implications of the isotopic ages of ignimbrite flows, Southern Atacama Desert, Chile. *Nature*, **215**(5102), 723–724.

Clark, A.H., Tosdal, R.M., Farrar, E. & Plazolles, V.A. (1990) Geomorphologic environment and age of supergene enrichment of the Cuajone, Quellaveco, and Toquepala porphyry copper deposits southern Peru. *Econ. Geol.*, **85**, 1604–1628.

Cornejo, P., Mpodozis, C., Ramírez, C. F. & Tomlinson, A. (1993). Estudio geológico de la región de Potrerillos y El Salvador (26°–27° Lat. S). Servicio Nacional de Geología y Minería (SERNAGEOMIN), Santiago, Chile, Registered Report IR-93-01.

Cornejo, P. & Mpodozis, C. (2015) Aptian (122-116 Ma) silver mineralization in extensión-related magmatism in the Domeyko Cordillera: the Caracoles district, northern Chile. XIV Congreso Geológico Chileno, La Serena.

Davis, W.M. (1905) The geographical cycle in an arid climate. *J. Geol.*, **13**, 381–407.

Dill, H.G. (2007) A review of mineral resources in Malawi: with special reference to aluminum variation in mineral deposits. *J. Afr. Earth Sc.*, **47**, 153–173.

Dilles, J., Tomlinson, A., García, M. & Alcota, H. (2011) The geology of the Fortuna Granodiorite Complex, Chuquicamata district, northern Chile: Relation to porphyry

copper deposits, *SGA Biennial Meeting, 11 th*, Antofagasta, 399–401.

Dohrenwend, J.C. & Parsons, A.J. (2009) Pediments in arid environments. *Geomorphology of Desert Environments*, pp. 377–411. Springer Science + Business Media B.V., Amsterdam, the Netherlands.

Dunai, T.J., Gónzalez-López, G.A., Juez-Larré, J. & Carrizo, D. (2005) Oligocene/Miocene age of aridity in the Atacama Desert revealed by exposure dating of erosion sensitive landforms. *Geology*, **33**, 321–324.

Emmons, W.H. (1917) The enrichment of ore deposits. *U.S. Geol. Surv. Bull.*, **625**, 530p.

Evenstar, L.A., Hartley, A.J., Stuart, F.M., Mather, A.E., Rice, C.M. & Chong, G. (2009) Multiphase development of the Atacama Planation Surface recorded by cosmogenic He-3 exposure ages: implications for uplift and Cenozoic climate change in western South America. *Geology*, **37**, 658–658.

Farías, M., Charrier, R., Comte, D., Martinod, J. & Hérail, G. (2005) Late Cenozoic deformation and uplift of the western flank of the Altiplano: evidence from the depositional, tectonic, and geomorphologic evolution and shallow seismic activity (northern Chile at 19°30′S). *Tectonics*, **24**. https://doi.org/10.1029/2004tc001667 (TC4001).

Fernández-Mort, A., Alonso-Zarza, A.M., Riquelme, R. & Campos, E. (2016) Origen y contexto sedimentario de depósitos de cobre exótico Cenozoicos del Desierto de Atacama, norte de Chile. *Geo-Temas*, **16**(1), 213–216.

Flower, B.P. & Kennett, J.P. (1994) The middle Miocene climatic transition; East Antarctic ice sheet development, deep ocean circulation and global carbon cycling. *Palaeogeogr. Palaeoclimatol. Palaeoecol.*, **108**(1994), 537–555.

Garcia, M., Riquelme, R., Farias, M., Herail, G. & Charrier, R. (2011) Late Miocene-Holocene canyon incision in the western Altiplano, northern Chile; 11 tectonic or climatic forcing? *J. Geol. Soc.*, **168**, 1–14.

Gehrels, G. (2010) Detrital Zircon U-Pb Geochronology: Current Methods and New Opportunities. In: *Recent Advances in Tectonics of Sedimentary Basins* (Ed. by C. Busby & A. Azor), pp. 47–62. Blackwell Publishing, Hoboken, NJ.

Gustafson, L.B. & Hunt, J.P. (1975) The porphyry copper deposit at El Salvador Chile. *Econ. Geol.*, **70**, 857–912.

Hartley, A.J. (2003) Andean uplift and climate change. *J. Geol. Soc.*, **160**, 7–10.

Hartley, A.J. & Chong, G. (2002) Late Pliocene age for the Atacama Desert: implications for the desertification of western South America. *Geology*, **30**, 43–46.

Hartley, A.J. & Rice, C.M. (2005) Controls on supergene enrichment of porphyry copper deposits in the Central Andes: a review and discussion. *Miner. Deposita*, **40**, 515–525.

Hinojosa, L.F. (2005) Cambios climaticos y vegetacionales inferidos a partir de paleofloras cenozoicas del sur de Sadamerica. *Rev. Geol. Chile*, **32**(1), 95–115.

Hinojosa, L.F. & Villagran, C. (2005) Did South American Mixed Paleofloras evolve under thermal equability or in the absence of an effective Andean barrier during the Cenozoic? *Palaeogeogr. Palaeoclimatol. Palaeoecol.*, **217**, 1–23.

Hogg, S. (1982) Sheetfloods, sheetwash, shetflow, or..? *Earth-Cience Rev.*, **18**, 59–76.

Horton, B.K. & Schmitt, J.G. (1996) Sedimentology of the lacustrine fan-delt'a system, Miocene Horse Camp Formation, Nevada, USA. *Sedimentology*, **43**, 133–155.

Jordan, T.E., Kirk-Lawlor, N., Blanco, N., Nester, P. & Rech, J. (2014) Landscape modification in response to repeated onset of hyperarid paleoclimate states since 14 Ma, Atacama Desert, Chile. *Geol. Soc. Am. Bull.*, **126**, B30978–B30971.

Kay, S.M., Godoy, E. & Kurtz, A. (2005) Episodic arc migration, crustal thickening, subduction erosion, and magmatism in the south-central Andes. *GSA Bull.*, **117**, 67–88.

Lamb, S. & Davis, P. (2003) Cenozoic climate change as a possible cause for the rise of the Andes. *Nature*, **425**, 792–797.

Lanphere, M.A. & Dalrymple, G.B. (2000) First-principles calibration of 38 Ar tracers: implications for the ages of ^{40}Ar/^{39}Ar fluence monitors. U.S. Geological Survey Professional Paper, 1621, 10 pp.

Layer, P.W. (2000) ^{40}Argon/ ^{39}Argon age of the El'gygytgyn impact event, Chukotka, Russia. *Meteorit. Planet. Sci.*, **35**, 591–599.

Li, J.-W. & Vasconcelos, P. (2002) Cenozoic continental weathering and its implications for the palaeoclimate: evidence from 40 Ar/ 39 Ar geochronology of supergene K-Mn oxides in Mt Tabor, central Queensland, Australia. *Earth Planet. Sci. Lett.*, **200**, 223–239.

Ludwig, K.R. (2008) Isoplot 3.6. *Berkeley Geochron. Ctr. Spec. Pub.*, **4**, 1–77.

Maksaev, V. & Zentilli, M. (1999) Fission track thermochronology of the Domeyko Cordillera, Northern Chile: implications for Andean tectonics and porphyry copper metallogenesis. *Explor. Min. Geol.*, **8**, 65–89.

Marinovic, N. & García, M. (1999) Hoja Pampa Unión, Región de Antofagasta. Escala 1:100.000, Servicio Nacional de Geología y Minería, Mapas Geológicos, N° 9, Santiago.

Marsh, T., Einaudi, M. & McWilliams, M. (1997) ^{40}Ar/^{39}Ar geochronology of Cu–Au and Au–Ag mineralization in the Potrerillos District, Chile. *Econ. Geol.*, **92**, 784–806.

May, G., Hartley, A., Chong, G., Stuart, F., Turner, P. & Kape, S. (2005) Eocene to Pleistocene lithoestratigraphy, chonostratigraphy and tectono-sedimentary evolution of the Calama Basin, northern Chile. *Rev. Geol. Chile*, **32**, 33–58.

Menzies, A., Campos, E., Hernández, V., Sola, S. & Riquelme, R. (2015) Understanding Exotic-Cu Mineralisation: Part II - Characterisation of Black Copper ("Cobre Negro"). 13th SGA Biennial Meeting, France.

Miall, A.D. (1977) A review of the braided river depositional environment. *Earth-Sci. Rev.*, **13**, 1–62.

Miall, A.D. (1996) *The Geology of Fluvial Deposits: Sedimentary Facies, Basin Analysis, and Petroleum Geology*, 582 pp. Springer, New York.

Mora, R., Artal, J., Brockway, H., Martínez, E. & Muhr, R. (2004) El Tesoro exotic copper deposit, Antofagasta Region, northern Chile. *Soc. Econ. Geol. Spec. Publ.*, **11**, 187–197.

Morandé, J. (2014) El basamento pre-Mesozoico de la Sierra Limón Verde: Implicancias para la evolución tectónica del norte de Chile. M. Sc. Thesis (Unpublished), Departamento de Geología, Universidad de Chile, 121 pp.

Mortimer, C. (1973) The Cenozoic history of the southern Atacama Desert, Chile. *Geol. Soc. London J.*, **129**, 505–526.

Mortimer, C. (1980) Drainage evolution of the Atacama Desert of northernmost Chile. *Rev. Geol. Chile*, **11**, 3–28.

Mote, T., Becker, T., Renne, P. & Brimhall, G. (2001) Chronology of exotic mineralization at El Salvador, Chile, by $^{40}Ar/^{39}Ar$ dating of copper wad and supergene alunite. *Econ. Geol.*, **96**, 351–366.

Mpodozis, C. & Cornejo, P. (2012) Cenozoic tectonics and porphyry copper systems of the Chilean Andes. *Soc. Econ. Geol. Spec. Publ.*, **16**, 329–360.

Mpodozis, C. & Perelló, J. (2003) Porphyry copper metallogeny of the middle-Eocene-early Oligocene arc of western South America. Relationships with volcanism and arc segmentation- In: X Congreso Geológico Chileno, Concepción, Extended Abstracts (CD), 1 p.

Mpodozis, C., Marinovic, N., Smoje, I. & Cuitiño, L. (1993) Estudio geológico-estructural de la Cordillera de Domeyko entre Sierra Limón Verde y Sierra Mariposa, Región de Antofagasta. Escala 1:100.000, Santiago, Chile, Servicio Nacional de Geología y Minería, Informe Registrado, IR-93-04, 282 p., Santiago.

Münchmeyer, C. (1996). Exotic deposits – products of lateral migration of supergene solutions from porphyry copper deposits. In: *Andean Copper Deposits: New Discoveries, Mineralization, Styles and Metallogeny* (Ed. by F. Camus, R. H. Sillitoe & R. Petersen) *Soc. Econ. Geol. Spec. Publ.*, **5**, 43–58.

Nalpas, T., Hérail, G., Mpodozis, C., Riquelme, R., Clavero, J. & Dabard, M.P. (2005) Thermochronological data and denudation history along a transect between Chañaral and Pedernales (~26° S), North Chilean Andes: Orogenic implications. In: International Symposium on Andean Geodynamics, 6 th, Barcelona, 548−551.

Nalpas, T., Dabard, M.-P., Ruffet, G., Vernon, A., Mpodozis, C., Loi, A. & Hérail, G. (2008) Sedimentation and preservation of the Miocene Atacama Gravels in the Pedernales–Chañaral Area, Northern Chile: Climatic or tectonic control? *Tectonophysics*, **259**, 161–173.

Nemec, W. & Steel, R.J. (1984) Alluvial and coastal conglomerates: their significant features and some comments on gravelly mass-flow deposits. In: *Sedimentology of Gravels and Conglomerates* (Ed. by E.H. Koster & R.J. Steel), *Canadian Society of Petroleum Geologists Memoir*, **10**, 1–31.

Niemeyer, H. & Urrutia, C. (2009) Transcurrencia a lo largo de la Falla Sierra de Varas (Sistema de fallas de la Cordillera de Domeyko), norte de Chile. *Andean Geol.*, **36**, 37–49.

Oerter, E., Amundson, R., Heimsath, A., Jungers, M., Chong, G. & Renne, P. (2016) Early to middle miocene climate in the atacama desert of Northern Chile. *Palaeogeogr. Palaeoclimatol. Palaeoecol.*, **441**, 890–900.

Olivares, B. (2001). Alzamiento, termocronometría y evolución tectónica de bloques en la Cordillera de Domeyko, Norte de Chile. M. Sc. Thesis (Unpublished), Departamento de Geología, Universidad de Chile, 70 pp.

de Oliveira Carmo, I. & Vasconcelos, P.M. (2006) 40Ar/39Ar geochronology constraints on late Miocene weathering rates in Minas Gerais, Brazil. *Earth Planet. Sci. Lett.*, **241**, 80–94.

Parnel, J., Mark, D.F., Frei, R., Fallick, A.E. & Ellam, R.M. (2014) 40 Ar/ 39 Ar dating of exceptional concentration of metals by weathering of Precambrian rocks at the Precambrian–Cambrian boundary. *Precambr. Res.*, **246**, 54–63.

Perelló, J., Muhr, R., Mora, R., Martinez, E., Brockway, H., Swaneck, T., Artal, J., Mpodozis, C., Münchmeyer, C., Clifford, J., Acuña, E., Valenzuela, D. & Argandoña, R. (2010) Wealth Creation through Exploration in a Mature Terrain: the Case History of the Centinela District, Northern Chile Porphyry Copper Belt. *Soc. Econ. Geol. Spec. Publ.*, **15**, 229–252.

Phillips, J.D. (2002) Erosion, isostatic response, and the missing peneplains. *Geomorphology*, **45**(2002), 225–241.

Quang, C.X., Clark, A.H., Lee, J.K.W. & Guillén, B.J. (2003) 40Ar–39Ar ages of hypogene and supergene mineralization in the Cerro Verde-Santa Rosa porphyry Co–Mo cluster, Arequipa, Peru′. *Econ. Geol.*, **98**, 1683–1696.

Quang, C.X., Clark, A.H., Lee, J.K.W. & Hawkes, N. (2005) Response of supergene process to episodic Cenozoic uplift, pediment erosion, and ignimbrite eruption in the porphyry copper province of Southern Perú. *Econ. Geol.*, **100**, 87–114.

Ransome, F.L. (1919) The copper deposits of Ray and Miami, Arizona. *U.S. Geol. Surv. Prof. Pap.*, **115**, 192p.

Rech, J.A., Currie, B.S., Michalski, G. & Cowan, M. (2006) Neogene climate change and uplift in the Atacama Desert, Chile. *Geology*, **34**, 761–764.

Rech, J.A., Currie, B.S., Shullenberger, E.D., Dunagean, S.P., Jordan, T.E., Blanco, N., Tomlinson, A.J., Rowe, H.D. & Houston, J. (2010) Evidence for the development of the Andean rain shadow from a Neogene isotopic record in the Atacama Desert, Chile. *Earth Planet. Sci. Lett.*, **292**, 371–382.

Reich, M., Palacios, C., Vargas, G., Luo, S., Cameron, E.M., Leybourne, M.I., Parada, M.A., Zúñiga, A. & You, C.-F. (2009) Supergene enrichment of copper deposits since the onset of modern hyperaridity in the Atacama Desert, Chile. *Minerallium. Deposita*, **44**, 497–504.

Reutter, K.-J., Scheuber, E. & Chong, G. (1996) The Precordilleran fault system of Chuquicamata, northern Chile: Evidence for reversals along arc-parallel strike-slip faults. *Tectonophysics*, **259**, 213–228.

Riquelme, R., Martinod, J., Hérail, G., Darrozes, J. & Charrier, R. (2003) A geomorphological approach to determining the Neogene to Recent tectonic deformation in the Coastal Cordillera of northern Chile (Atacama). *Tectonophysics*, **361**, 255–275.

Riquelme, R., Hérail, G., Martinod, J., Charrier, R. & Darrozes, J. (2007) Late Cenozoic geomorphologic signal of Andean forearc deformation and tilting associated with the uplift and climate changes of the Southern Atacama Desert (26°S-28°S). *Geomorphology*, **86**, 283–306.

Rodriguez, M.P., Carretier, S., Charrier, R., Saillard, M., Regard, V., Herail, G., Hall, S., Farber, D. & Audin, L. (2013) Geochronology of pediments and marine terraces in north-central Chile and their implications for Quaternary uplift in the Western Andes. *Geomorphology*, **180**, 33–46.

Sáez, A., Cabrera, L., Jensen, A. & Chong, G. (1999) Late Neogene lacustrine record and paleogeography in the Quillagua-Llamara basin, Central Andean fore-arc (northern Chile). *Palaeogeogr. Palaeoclimatol. Palaeoecol.*, **151**, 5–37.

Sáez, A., Cabrera, L., Garcés, M., van den Bogaard, P., Jensen, A. & Gimeno, D. (2012) The stratigraphic record of changing hyperaridity in the Atacama Desert over the last 10 Ma. *Earth Planet. Sci. Lett.*, **355–356**, 32–38.

Sanchez, C., Brichau, S., Riquelme, R., Lopez, C., Campos, E., Farias, M., Mpodozis, C., Regard, V. & Herail, G. (2015) Low temperature thermochronology, porphyry-Cu exhumation history and supergene enrichment in the Centinela District, Atacama Desert, Chile. XIV Congreso Geológico Chileno, La Serena, Extended Abstracts (CD), 1 pp.

Sillitoe, R. (2005) Supergene Oxidized and Enriched Porphyry Copper and related Deposits. Economic Geology 100 th Anniversary Volume, 723–768.

Sillitoe, R. (2010) Porphyry copper systems. *Econ. Geol.*, **105**, 3–41.

Sillitoe, R. & McKee, H. (1996) Age of supergene oxidation and enrichment in the Chilean porphyry copper province. *Econ. Geol.*, **91**, 164–179.

Sillitoe, R.H. & Perelló, J. (2005) Andean copper province: Tectonomagmatic settings, deposit types, metallogeny, exploration, and discovery. Economic Geology 100 th Anniversary Volume, 845-890.

Sillitoe, R.H., Mortimer, C. & Clark, A.H. (1968) A chronology of landform evolution and supergene mineral alteration, southern Atacama Desert, Chile. *Trans. Inst. Min. Metall. (Sect. B: Appl. Earth sci.)*, **77**, B166–B169.

Smith, G.A. (1986) Coarse-grained nonmarine volcaniclastic sediment: terminology and depositional process. *Geol. Soc. Am. Bull.*, **97**, 1–10.

Spier, C.A., Vasconcelos, P.M. & Oliviera, S.M.B. (2006) 40 Ar/ 39 Ar geochronological constraints on the evolution of lateritic iron deposits in the Quadrilátero Ferrífero, Minas Gerais, Brazil. *Chem. Geol.*, **234**, 79–104.

Stern, C.R. (2004) Active Andean volcanism: its geologic and tectonic setting. *Rev. Geol. Chile*, **31**, 161–206.

Strudley, M.W. & Murray, A.B. (2007) Sensitivity analysis of pediment development through numerical simulation and selected geospatial query. *Geomorphology*, **88**, 329–351.

Svendsen, J., Stollhofen, H., Krapf, C.B.E. & Stanistreet, I.G. (2003) Mass and hyperconcentrated flow deposits record dune damming and catastrophic breakthrough of ephemeral rivers, Skeleton Coast Erg, Namibia. *Sediment. Geol.*, **160**, 7–31.

Tapia, M., Riquelme, R., Marquardt, C., Mpodozis, C. & Mora, R. (2012) Estratigrafía y sedimentología de la Cuenca El Tesoro, Distrito Centinela (región de Antofagasta) y su relación con la mineralización exótica de cobre. In: XIII Congreso Geológico Chileno, Antofagasta.

Tomlinson, A.J. & Blanco, N. (1997a) Structural evolution and displacement history of the West fault system, Precordillera, Chile: Pt. 1. Synmineral history. In: VIII Congreso Geológico Chileno, Antofagasta, 3, 1873–1878.

Tomlinson, A.J. & Blanco, N. (1997b) Structural evolution and displacement history of the West fault system, Precordillera, Chile: Pt. 2. Postmineral history. In VIII Congreso Geológico Chileno, Antofagasta, 3, 1878–1882.

Tomlinson, A.J., Dilles, J.H. & Maksaev, V. (2001) Application of apatite (U-Th)/He thermochronometry to the determination of the sense and amount of vertical fault displacement at the Chuquicamata porphyry copper deposit, Chile—a discussion. *Econ. Geol.*, **96**, 1307–1309.

Tosdal, R.M. (1978) The timing of the geomorphic and tectonic evolution of the southernmost Peruvian Andes. Unpublished M.Sc. thesis, Kingston, Ontario, Queen's University, 136 pp.

Truswell, E.M. (1993) Vegetation changes in the Australian Tertiary in response to climatic and phytogeographic forcing factors. *Aust. Syst. Bot.*, **6**(1993), 533–557.

Uba, C.E., Heubeck, C. & Hulka, C. (2005) Facies analysis and basin architecture of the Neogene Subandean synorogenic wedge, southern Bolivia. *Sediment. Geol.*, **180**, 91–123.

Vasconcelos, P.M. (1999) K–Ar and $^{40}Ar/^{39}Ar$ geochronology of weathering processes. *Annu. Rev. Earth Planet. Sci.*, **27**, 183–229.

Vasconcelos, P.M., Reich, M. & Shuster, L. (2015) The paleoclimatic signatures of supergene metal deposits. *Elements*, **11**, 317–322.

Waresback, D.B. & Turbeville, B.N. (1990) Evolution of a Plio-Pleistocene volcanogenic–alluvial fan: the Puye Formation, Jemez Mountains, NewMexico. *Geol. Soc. Am. Bull.*, **102**, 298–314.

de Wet, C.B., Godfrey, L. & Andrew, P. (2015) Sedimentology and stable isotopes from a lacustrine-to-palustrine limestone deposited in an arid setting, climatic and tectonic factors: Miocene-Pliocene Opache Formation, Atacama Desert, Chile. *Palaeogeogr. Palaeoclimatol. Palaeoecol.*, **426**, 46–67.

Yanites, B.J. & Kesler, S.E. (2015) A climate signal in exhumation patterns revealed by porphyry copper deposits. *Nat. Geosci.*, **8**, 462–465.

Zachos, J., Pagani, M., Sloan, L., Thomas, E. & Billups, K. (2001) Trends, rhythms and aberrations in global climate 65 Ma to present. *Science*, **292**, 686.

Manuscript received 30 January 2016; In revised form 18 July 2017; Manuscript accepted 21 July 2017.